EURISOL DS Project

TASK 7: Proton Accelerator design

Deliverable D3 - Low- and Medium-β linac

Layout and beam dynamics report

Planned Date (month): **54**

Achieved Date (month): **6/2009**

Lead Contractor(s): **P3-INFN**

Project acronym: *EURISOL DS*

Project full title: *EUROPEAN ISOTOPE SEPARATION ON-LINE*
                          RADIOACTIVE ION BEAM FACILITY

Start of the Project: *1st February 2005*
Duration of the project: *54 months*

RIDS 515768 TASK: 7	DATE: 3/2009	
DELIVERABLE: D3-LOW- AND MEDIUM-β LINAC	PAGE 1	

EURISOL Driver - Injector and Superconducting Low-β linac section

Authors:

A. Facco, A. Balabin, Ma Yanyun, R. Paparella, D. Zenere, INFN-Laboratori Nazionali di Legnaro, Padova, Italy; D. Berkovits, J. Rodnizki, SOREQ, Yavne, Israel; J. L. Biarrotte, S. Bousson, A. Ponton, G. Olry, IPN Orsay, France; R. Duperrier, D. Uriot, CEA/Saclay, France; V. Zvyagintsev, TRIUMF, Vancouver, Canada.

Abstract

The present document describes the Low- and Medium-β section of the EURISOL DS Driver Accelerator. This section consists of a superconducting linac, based on Half-Wave (HWR) and SPOKE type resonators, preceded by a short, normal-conducting MEBT (Medium Energy Beam Transport) section that performs input beam matching. The scope of this linac is to bring the beams of H^-, D^+ and $^3He^{++}$ produced by the Ion Injector (Deliverable D-5) to the energy and beam parameters required for injection in the superconducting High-β linac (Deliverable D4-High β linac).

The present beam dynamics design reaches the goal of accelerating the required high current beams to the design energy (about 100 MeV/A, depending on the ion species), with minimum emittance growth and with low losses, using realistic and cost-effective, although innovative, technological solutions.

The Low- and Medium-β linac layout is described, together with the fundamental parameters and characteristics of its components and the system performance.

1. Introduction

The Low and medium-β linac section (LMB) is the part of the EURISOL Driver which must accelerate the H^-, D^+ and $^3He^{++}$ beams produced by the Ion Injector (see Deliverable D5) to the energy and beam parameters required by the High-β Linac (see Deliverable D4) [1].

It includes the following main sub-sections:

1.   Medium-Energy Beam Transport (MEBT)

2. $\beta=0.09$ Half-Wave Resonators section (HWR1)

3. $\beta=0.15$ Half-Wave Resonators section (HWR2)

4. $\beta=0.3$ Triple-SPOKE Resonators linac (SPOKE)

The Low- and Medium-β linac design was driven by the EURISOL-DS requirement of a fully superconducting driver linac [2], and by the specific experience in the field developed by EURISOL DS participants and contributors in the EURISOL-DS Task 8 and in other projects. The linac scheme is the ISCL (Independently-phased SuperConducting Linac) one, based on a large number of short resonators with large velocity acceptance, which takes two main advantages:

1) the linac allows to modify the beam velocity profile, thus acceleration at maximum gradient of particles in a wide range of A/q;

2) in case of failure of a limited number of resonators, the linac can be often operated anyhow, with a modified beam dynamics.

A conservative design gradient, or the presence of spare-on-line, can prevent loss of performance in case of resonator failure. This is not allowed by normal-conducting Drift-Tube Linacs, where one cavity failure or underperformance is not compatible with operation.

RIDS 515768 TASK: 7	DATE: 3/2009	
DELIVERABLE: D3-LOW- AND MEDIUM-β LINAC	PAGE 4	

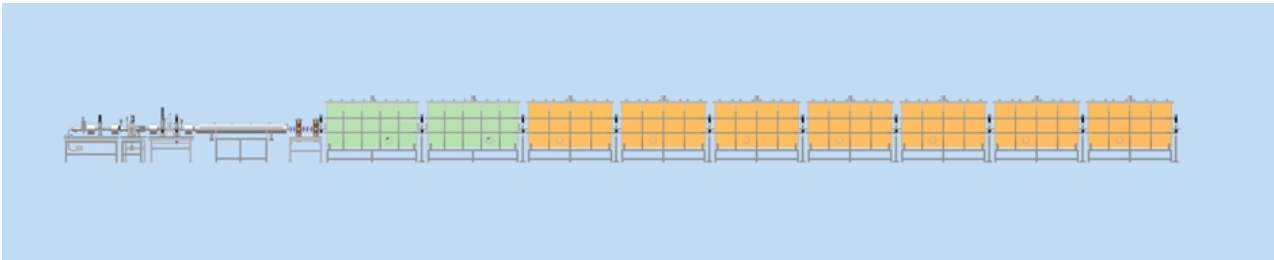Figure 1.1. Side view of the first part of the EURISOL Driver, with the Ion Injector and the superconducting Low-β linac section.

The main LMB requirements are low losses, low emittance growth, high acceleration efficiency.

The HWR1 and HWR2 subsections are based on superconducting Half-Wave Resonators (HWR). The design of this part of the linac have important similarities with the 40 MeV/A SARAF linac under construction at SOREQ (Israel) [3], in the general concept and in the cryomodule technology. For the EURISOL LMB, however, excellent output beam quality is a dominant requirement over high acceleration efficiency, in order to prevent halo formation that would cause beam losses at high energy in the subsequent High-β section. For this reason, two important modifications were made to the SARAF design: 1) a MEBT section was introduced both for matching the RFQ beam to the linac and for eliminating at low energy all the particles from the RFQ that would be eventually lost in the linac; 2) the first two β=0.09 HWR cryostats were modified, resembling the layout proposed also in the IFMIF linac [4]. Moreover, a different HWR design was proposed in order to increase mechanical stability of present SARAF resonators.

The β=0.3 section is based on Triple-Spoke resonators, not yet used in real accelerators until now, but successfully developed in the EURISOL-DS Task 8 framework and in other projects [5].

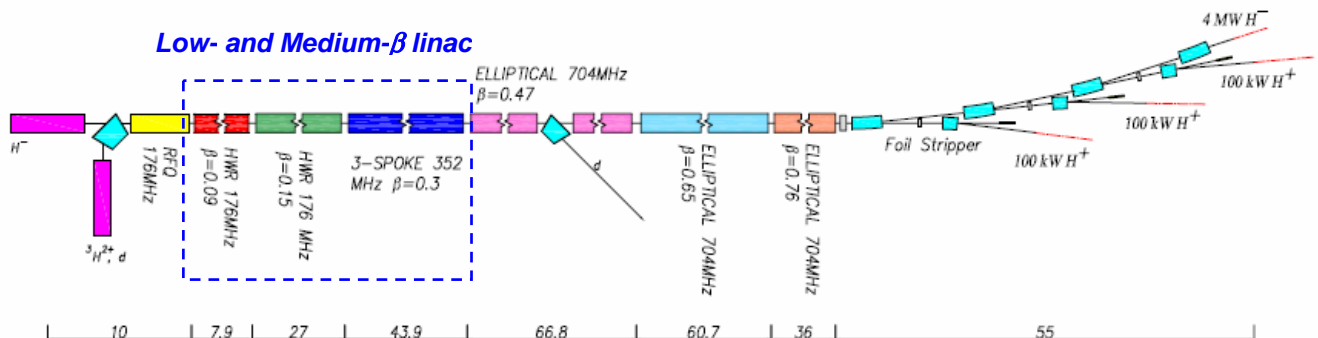| **RIDS 515768**	**TASK: 7**	**DATE:** **3/2009**	
DELIVERABLE: **D3-LOW- AND MEDIUM-β LINAC**		**PAGE** 5	

Figure 1.2 Schematic layout of the EURISOL Driver accelerator (not to scale), with the Low- and Medium-β linac (highlighted in the blue square) and its main subsections: HWR1 (red), HWR2 (green) and SPOKE (blue).

The novel high energy beam splitting scheme [27] introduced in EURISOL (Deliverable D6 - High Energy Beam Transport) imposed the capability of accelerating both negative and positive ions. This did not put particular requirements to this linac section, except for the use of bipolar power supplies in the quadrupole magnets. The beam diagnostics must be of course efficient for both types of beams.

All components proposed in this LMB design, although state of the art in accelerator technology, are either commercially available or similar to components which have been already developed by EURISOL participants or contributors, in order to reduce risks connected with R&D programs. The resonators have been especially developed for this project in the EURISOL Task 7 and Task 8 frameworks. Technological specifications (accelerating gradients, magnetic fields, alignment tolerances) have been chosen with conservative values rather than challenging ones.

In a previous design of the driver [28], a 352 MHz linac, which included a 6 MeV RFQ, was used for protons only (see Deliverables D1-Proton source and LEBT tests and D2-RFQ and MEBT) and

RIDS 515768	TASK: 7	DATE: 3/2009	
DELIVERABLE: D3-LOW- AND MEDIUM-β LINAC		PAGE 6	

a second 176 MHz ion injector, consisting of ion source, RFQ and low-β linac, was required just for ^{3}He and deuteron beams. In the present design, with rf frequency of 176 MHz in the first three sections, acceleration with superconducting cavities can start at 1.5 MeV/A for all beams, and only one and low beta linac with a short RFQ is required. This change led to a substantial simplification of the driver in the layout, in the components and in the operation procedures, and to a reduction of its cost.

RIDS 515768	TASK: 7	DATE: 3/2009	
DELIVERABLE: D3-LOW- AND MEDIUM-β LINAC		PAGE 7	

2. Linac specifications

The LMB front end is connected with the RFQ output flange of the Ion Injector; the high energy end is connected to the first quadrupole magnet of the High-β section.

The main LMB input and output beam specifications (Table 2.1) are dictated by the Ion Injector output beam characteristics and by the input beam requirements of the High-β linac section.

Table 2.1. Input and output beam specifications of the Low- and medium-β linac section.

Beams			H^-	D^+	$^3He^{++}$
current (emA)			5	5	0.1
A/q			1	2	3/2
Bunch Frequency (MHz)			176		
Duty cycle			cw		
Possibility of pulsed operation			Y		
Pulse length (μs)			>100		
Pulse Risetime/falltime (μs)			<20		
Pulse frequency (Hz)			<1000		
Input beam characteristics					
Energy (MeV/A)			1.5		
rms emittance		ε_x	<0.2	<0.2	<0.2
		ε_y	<0.2	<0.2	<0.2
(π mm mrad)		ε_z	<0.2	<0.2	<0.4
Output beam characteristics					
Energy (MeV/A)			> 60		
rms emittance		ε_x	<0.25	<0.25	<0.25
		ε_y	<0.25	<0.25	<0.25
(π mm mrad)		ε_z	<0.25	<0.25	<0.4
max beam losses total (W/m)			1	1	1

3. Layout and beam line components

3.1 Linac layout

The linac schematic layout is shown in Fig. 3.1, and the main beam transport elements in the different subsections are listed in Table 3.1.
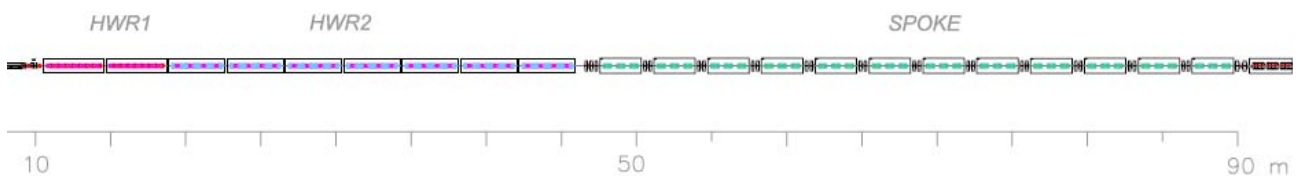

Figure 3.1 Low- and Medium-β linac schematic layout. The scale origin is located at the beginning of the Ion Injector (see Deliverable D5).

Table 3.1. Main linac sections and their beam transport elements.

	MEBT	HWR1	HWR2	SPOKE	total
n. NC cavities	2	-	-	-	2
n. SC cavities	-	16	56	36	110
n. cryostats	-	2	7	12	21
n. quad. magnets	5	-	-	25	30
n. SC solenoids	-	16	28	-	44
n. steerers (H+V)	2	4	14	12	32
n. BPMs	2	4	14	12	32
Length (m)	1.5	8.3	27.1	43.7	80.5

3.2 MEBT

The MEBT has the function of matching all different beams to the superconducting linac in different configurations. It includes 5 short quadrupole magnets and 2 normal-conducting bunchers with β_0=0.056 (the RFQ output beams velocity). A 177 mm long box at the end of the section is available for diagnostics.
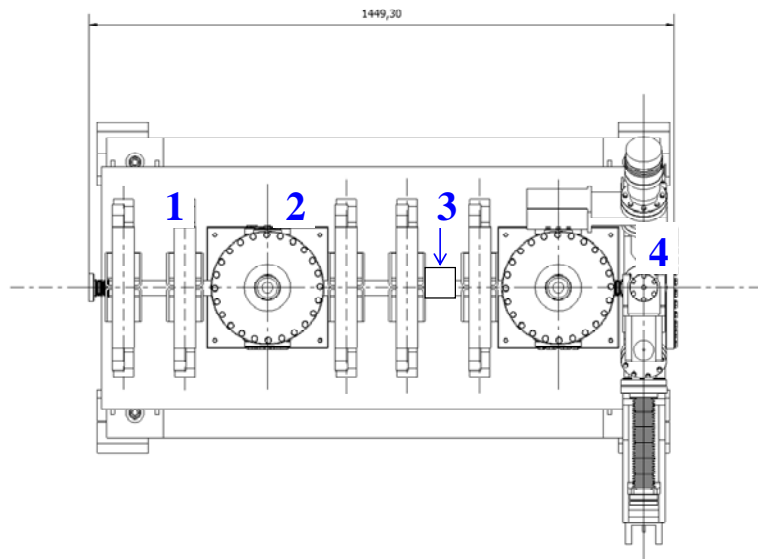

Figure 3.2. MEBT schematic layout. 1) quadrupole magnet with steerers; 2) buncher resonators; 3) beam position monitor (BPM); 4) Beam diagnostics box.

Another function of the MEBT is to stop the transmitted, but not accelerated particles from the RFQ. These particles hit the MEBT walls in different positions, due to the dependence of the quadrupole focusing strength on beam velocity. A water cooled, 5 mm radius diaphragm just before the first cryostats allows the final cleaning of the beam from the outer particles, limiting halo formation and emittance growth in the subsequent linac sections. The expected beam power losses in the MEBT are of the order of a few Watts in normal operation conditions, but can significantly increase in case of failure.
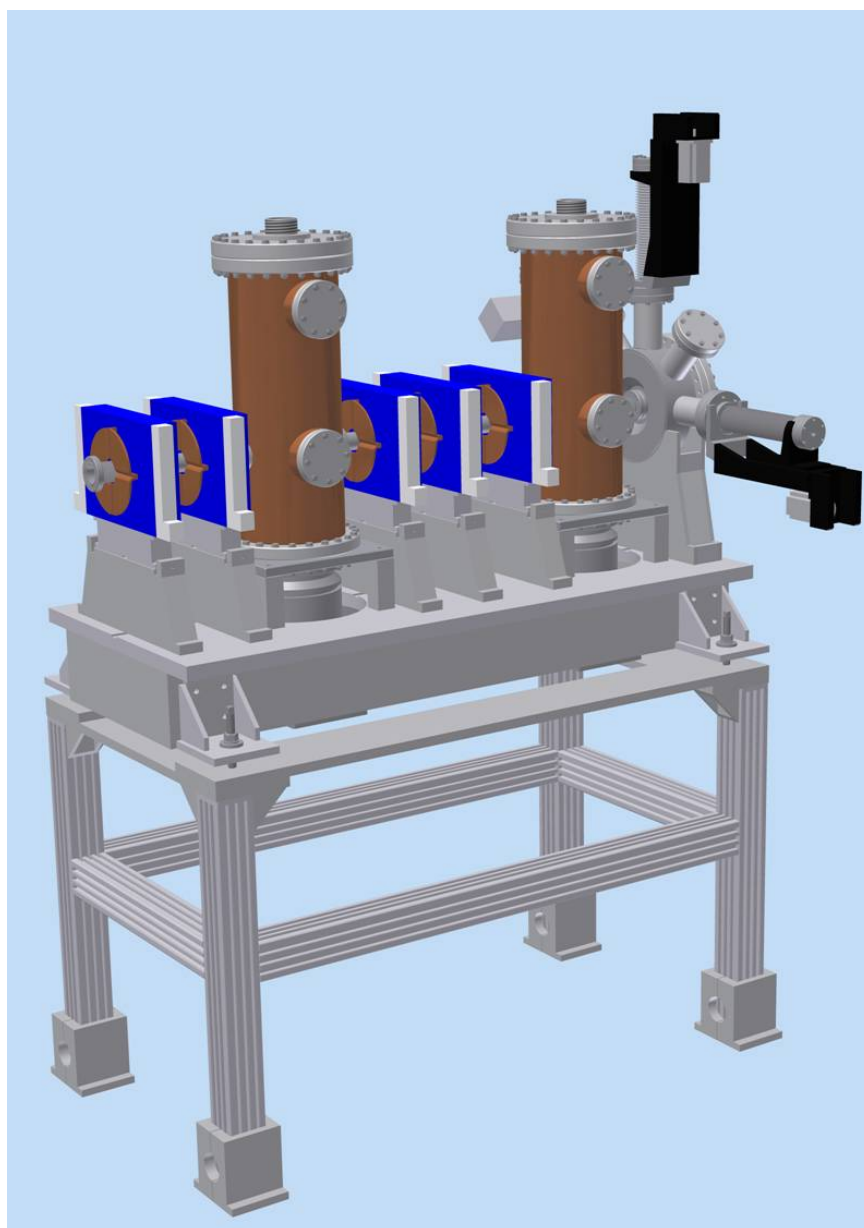
Figure 3.3. 3D view of the EURISOL MEBT.

RIDS 515768	TASK: 7	DATE: 3/2009	
DELIVERABLE: D3-LOW- AND MEDIUM-β LINAC		PAGE 11	

3.2.1 Quadrupole magnets

The MEBT quadrupoles must be operated at a maximum gradient of about 30 T/m with the deuteron beam. A 20% margin must be kept in the magnet specifications, leading to 36 T/m. Horizontal and vertical dipole correctors are integrated in the first and in the last quadrupoles, as for the SNS MEBT. The maximum required dipole field integral is 1 mT·m.

Table 3.2 MEBT quadrupole magnets specifications

N. of quadrupoles		5
Length	mm	70
Aperture diameter	mm	38
Max. gradient	T/m	36
Max steerer B integral	T·m	10^{-3}

3.2.2 Buncher cavities

The MEBT bunchers are 176 MHz resonators with 30 mm aperture diameter. Since the beam velocity at the RFQ output is fixed, large velocity acceptance is not required, but only acceleration efficiency and negligible steering at $\beta=0.056$. The relatively low accelerating field requirements allow the use of the normal conducting resonators technology, which is also the preferred choice in the MEBT section where beam losses are foreseen. The maximum required acceleration voltage is 200 kV for the D beam. A 20% margin has to be included in the cavity specifications.

Table 3.3. MEBT Bunchers effective acceleration voltage $V_{acc} = \Delta E_{max}/q$ for different beams.

cavity #	unit	H⁻	D⁺	³He⁺⁺
buncher 1	*kV*	50	100	80
buncher 2	*kV*	110	200	130

Table 3.4. MEBT Bunchers main specifications.

N. of bunchers		2
Length	*mm*	220
Aperture diameter	*mm*	30
Beam velocity β		0.056
Max. acceleration	*kV*	240
Max rf power	*kW*	15

3.2.3 Beam diagnostics

A beam position monitor is located before the 5th quadrupole, to guide the 1st steerer in centering the beam. A beam diagnostics box, that includes transverse and longitudinal beam profile measurements for the MEBT set up, a removable 5 mm radius diaphragm and a Faraday cup for beam current measurements, is located after the 2nd buncher in front of the 1st cryostat.

3.3 Low-β linac

The low-β linac includes 9 cryomodules containing 2-gap superconducting Half-Wave Resonators and superconducting solenoids. One beam position monitor and two pairs of horizontal and vertical steerers are mounted inside every cryostat for beam trajectory correction. Beam diagnostics boxes are located between neighbouring cryostats, and at the end of the section.

According to the beam dynamics specifications, the HWR cryomodules layouts are of two different types for the β=0.09 and for the β=0.16 resonators (see Figure 3.4 and 3.5). Horizontal and vertical steerers, integrated in two of the solenoids of each cryostat, to correct beam steering caused mainly by solenoid misalignment. A short beam position monitor is positioned after the 5th resonator, near the center of the cryostat, to to guide the settings of the steerer located in the 1st solenoid. The second pair of steerers is guided by the diagnostics box following the cryostat.

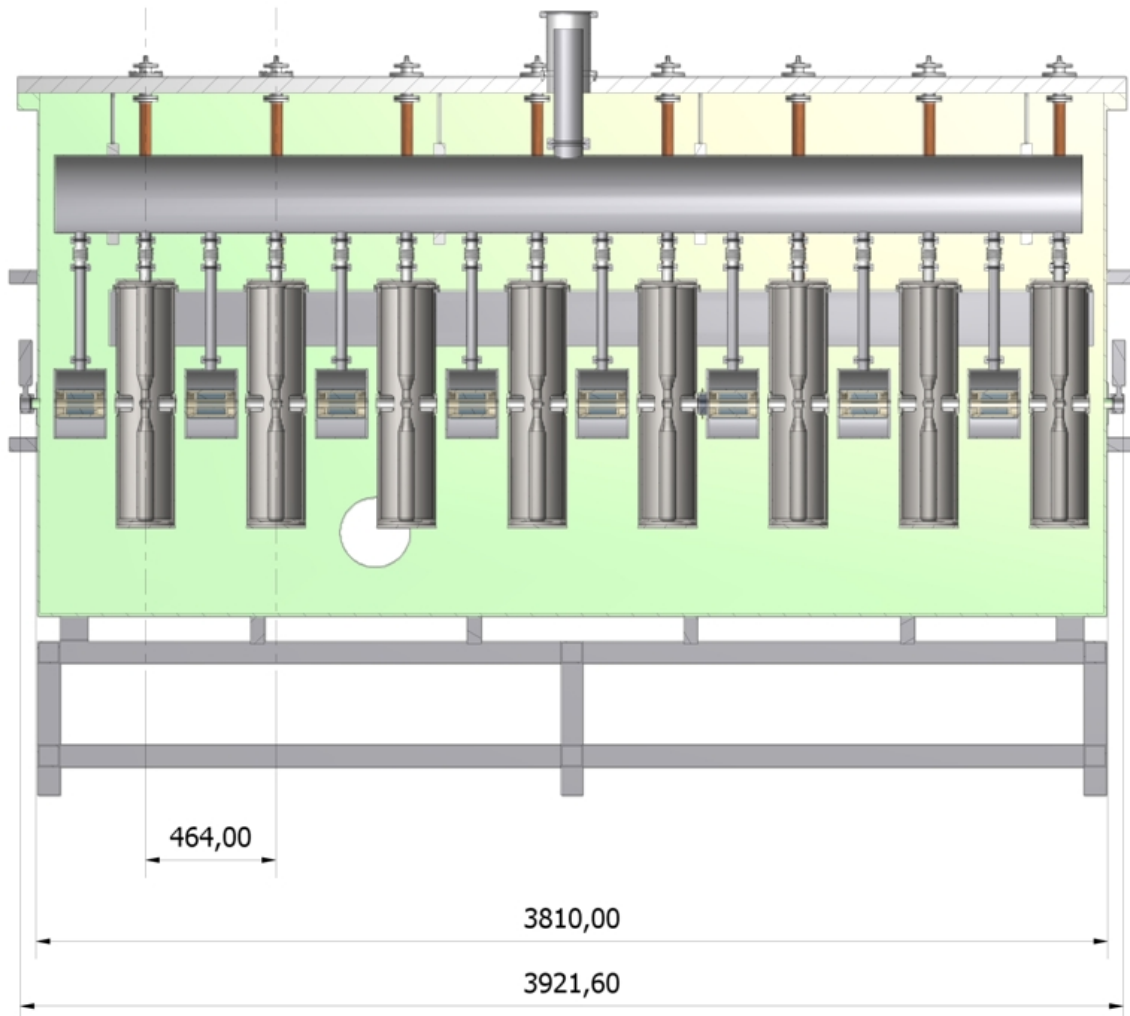Figure 3.4. β=0.09 cryostats schematic layout (dimensions in mm). The lower β cryostat includes 8 HWRs and 8 superconducting solenoids. The 1st and the 6th solenoids contain beam steerers. The short beam position monitor is located in front of the 5rd solenoid.
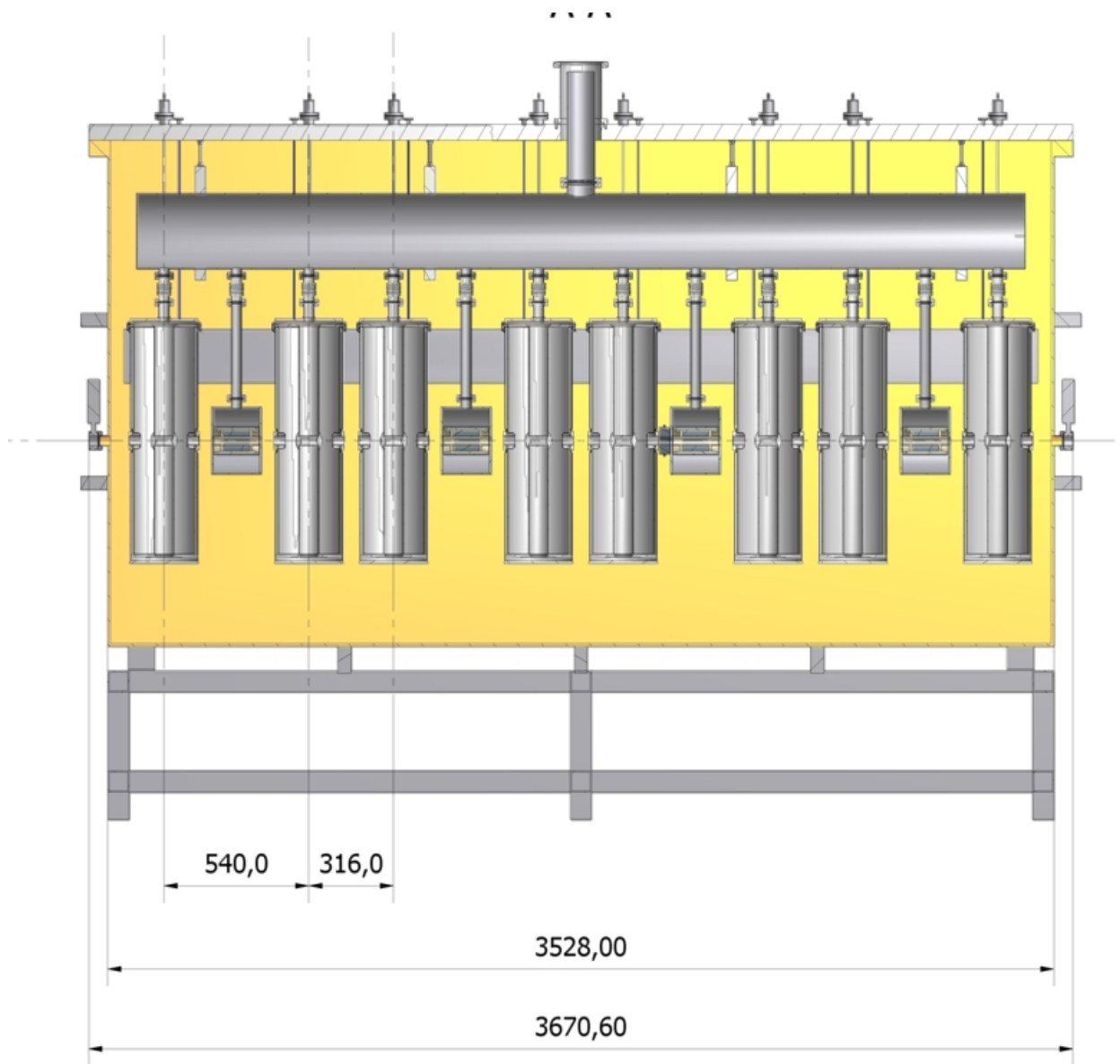
Figure 3.5. As in Fig. 3.4, for the β=0.16 cryostat. The higher β cryomodule still hosts 8 HWRs but only 4 SC solenoids, the 1st and the 3rd ones with integrated steerers. The short beam position monitor is located in front of the 3rd solenoid.

3.2.2 Superconducting resonators

Ths superconducting resonators are 2-gap ones of the Half-Wave type, characterized by large velocity acceptance and no beam steering effect. Their main requirements are listed in table 3.5.

Table 3.5. Superconducting resonators main specifications.

Element	units	HWR1	HWR2
Length	mm	220	300
Total aperture	mm	30	30
Rf frequency	MHz	176	176
Optimum β		0.09	0.16
Max. physical length	m	0.22	0.3
Nominal operation gradient	MV/m	4.7	5.2
Max. beam loading	kW	5	6
Max. rf power requirements	kW	6.25	7.5

3.2.3 Superconducting solenoids

The superconducting solenoids specifications are listed in table 3.6. Two solenoids per cryostat must include vertical and horizontal steerers.

Table 3.6. Superconducting solenoids specifications.

Element	units	Solenoid	Steerers
Length	mm	208	208
Total beam aperture	mm	38	38
Max. field B	T	6	-
Max field Integral	T·m	1	10^{-2}

3.2.3 HWR1 and HWR2 Beam diagnostics

Beam position and beam phase monitors, with aperture is 30 mm diameter and minimum resolution of 0.1 mm and 1 degree, respectively, are required for beam set-up and monitoring.
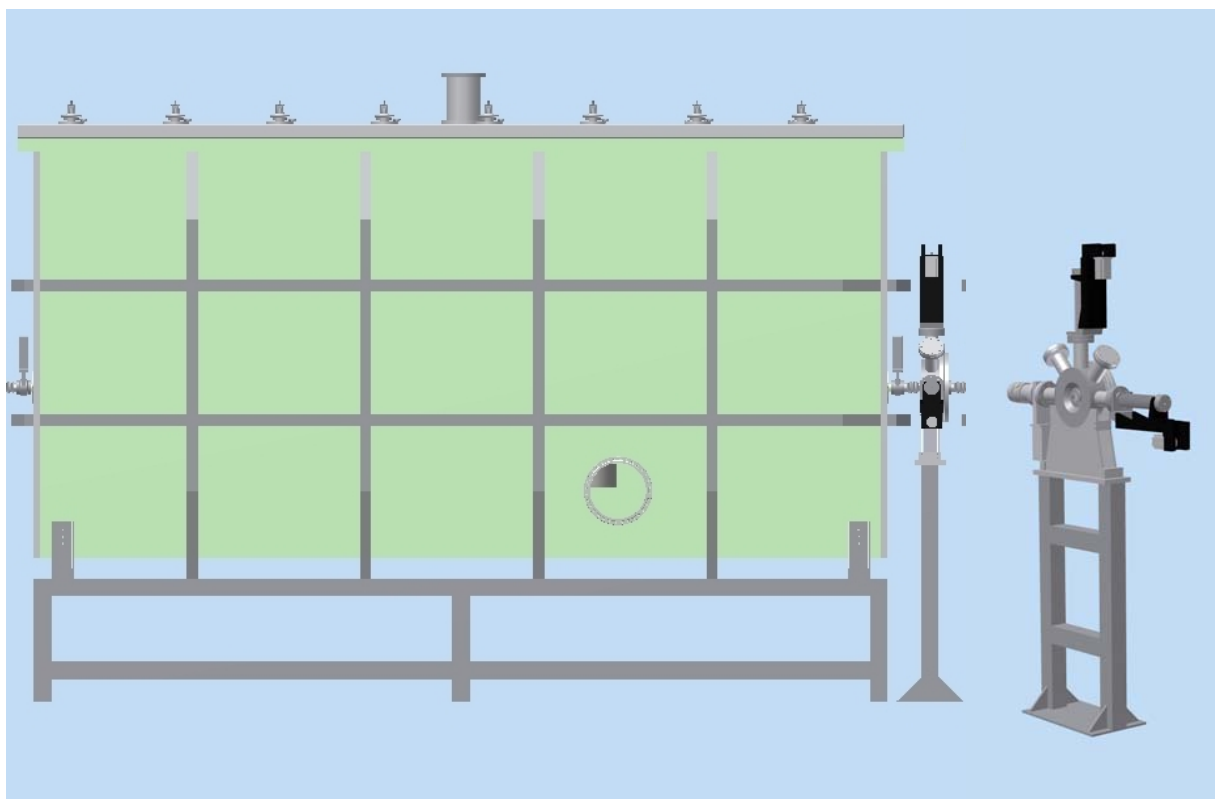
Figure 3.6. Left: side view of one low-β cryomodule, including one cryostat and one diagnostics box. Right: model of the diagnostics box with its support.

These requirements can be fulfilled by resonant stripline BPMs [7]. These devices are very compact and they can also be integrated with SC solenoids beam pipes and in the short spaces between solenoids and HWRs.

BPMs must be located also in the diagnostic boxes between cryostats, together with wire scanners giving the beam profile, and detectors for longitudinal beam profile measurement. The last box of the low-β line is located in the 330 mm drift at the end of the section, and contains an additional Faraday cup for beam current measurement in low duty cycle pulsed mode.

3.3 Medium-β linac

The medium-β linac consists of 12 cryomodules, each housing 3 superconducting Triple-Spoke resonators with β=0.3 working at 352 MHz [8]. Differently from the previous section, focusing is provided by room temperature quadrupole doublets located between neighbouring cryostats.
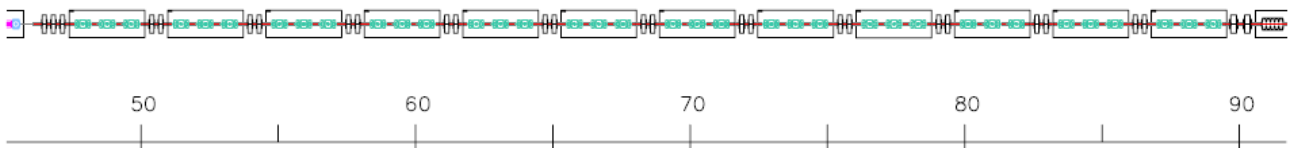

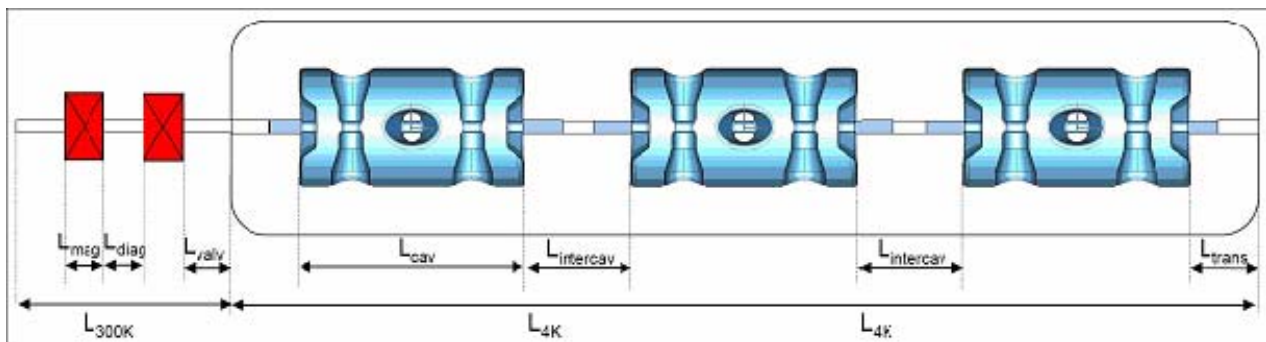Figure 3.7. Medium-β linac schematic layout with the elements position along the linac.

Figure 3.8. Schematic layout of the β=0.3 cryomodule containing Spoke cavities. L_{mag}=200 mm; L_{diag}=130 mm; L_{trans}=223 mm; L_{cav}=538 mm; $L_{intercav}$=346 mm; L_{300K}=850 mm; L_{4K}=1868 mm.

Beam diagnostics boxes are located between the two quadrupole magnets of each doublet, and contain wire scanner beam profile monitors, stripline beam position monitors/phase detectors.

At the beginning of the SPOKE section a triplet is required in order to provide transverse matching between two different lattices. This is obtained by adding one more quadrupole to the first doublet.

3.3.1 Superconducting resonators

Table 3.7. Superconducting resonators main specifications

Element	units	Triple-Spoke
Length	mm	716
Total aperture	mm	50
Rf frequency	MHz	352
Optimum β		0.3
Nominal operation gradient	MV/m	5.8
Rf power at 4.2 K	W	<10
Max. beam loading	kW	20
Max. rf power requirements	kW	25

The Triple Spoke, 4-gap resonators provide large acceleration and sufficient velocity acceptance for efficient acceleration up to the required 130 MeV/A for protons. As for HWRs, the accelerating gradient has been set to a somehow conservative value.

3.3.3 Quadrupole magnets

The quadrupole magnets and the steerers of the SPOKE section are standard, commercially available ones. Their main specifications are listed in Table 3.8.

Table 3.8. Medium-β magnetic elements specifications.

Element		quadrupoles	steerers
Length	mm	200	100
Aperture diameter	mm	60	60
Max. gradient	T/m	20	-
Max B integral	T·m	4	10^{-3}

3.2.3 SPOKE section beam diagnostics.

Beam diagnostics boxes are located between two quadrupole magnets, and include stripline BPMs and phase detectors with aperture diameter 60 mm, position and phase resolution of 0.1 mm and 1 deg, respectively. Wire scanners giving the beam profile are also present.

4. Beam dynamics

The LMB linac beam dynamics was studied with the TraceWin code [11]. The HWR section was previously studied also with the codes TRACK [12] and GPT [13] using the SARAF lattice [15]. The study included:

- design and optimization of the linac layout and definition of the linac components;
- calculation of the linac performance by means of multiparticle simulation with realistic fields;
- preliminary evaluation of beam losses;
- introduction of realistic errors in the linac and definition of a correction system.

Table 4.1. LMB linac main components and characteristics summary.

Linac section		MEBT	HWR1	HWR2	SPOKE
Cavity type		NC QWR	SC HWR	SC HWR	Triple-SPOKE
Optimum β		$\beta=0.056$	$\beta=0.09$	$\beta=0.16$	$\beta=0.3$
Cavity nominal E_a		1	4.7	5.2	5.8
Aperture radius	mm	15	15	15	25
n. cryostats		-	2	7	12
n. resonators /cryostat		-	8	8	3
n. resonators total		2	16	56	36
n. SC		-	8	4	-
Solenoids nominal B	T	-	6	6	-
n. quadrupole		5	-	-	25
Quad max gradient	T/m	36	-	-	20
H-V steerers		2	4	14	12
Steerer type		In quadrupoles	In solenoids	In solenoids	external
Steerers max B	T·m	10^{-3}	10^{-2}	10^{-2}	10^{-3}

4.1 Design criteria

In the LMB beam dynamics design, some main guidelines have been followed in order to obtain efficient acceleration with low emittance growth and little halo formation [14] [18]:

- Phase advance per period: its value for zero current was maintained below 90° in the transverse planes to avoid envelope instabilities.
- Longitudinal/Transverse phase advance ratio: this value was maintained as much as possible below 2, to avoid resonance between longitudinal and transverse phase space planes.
- In the HWR linac, the sign of the field in subsequent solenoids was alternated to partially cancel the x-y planes mixing.
- The phase advance per period was changed smoothly along the linac to avoid emittance growth.
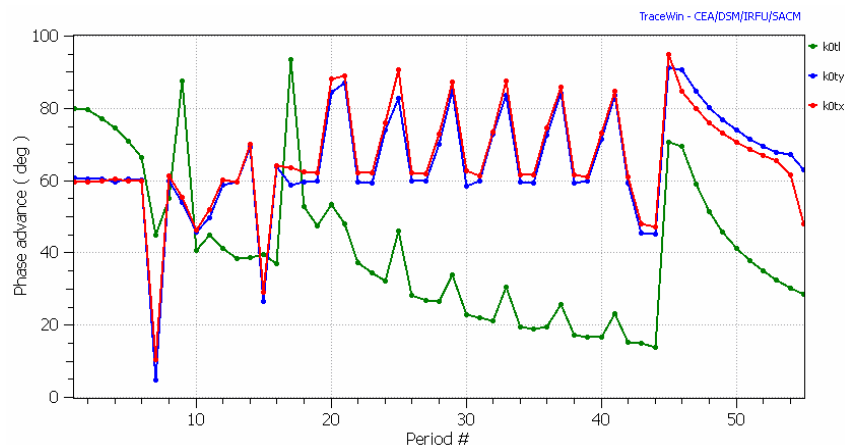
Figure 4.1. Phase advance per period vs. period number for the H⁻ beam.

To adjust the 6 Twiss parameters for a good matching at the linac input, a MEBT with 2 bunchers and 5 quadrupoles was necessary. The 1st quadrupole is mainly required to contain the RFQ output beam, strongly diverging in the x plane and converging in the y plane.

In the first 2, β=0.09 cryostats (1 solenoid + 1 HWR per period) the synchronous phase was set at -40 degrees and the accelerating field of the first few cavities had to be limited in order to maintain the phase advance specifications. This allowed transport with low emittance growth in the critical 1.5-9.2 MeV range also with H$^-$ beam, where space charge effects are more pronounced. The synchronous phase could be increased to -25 deg in the β=0.16 HWR section (1 HWR + 1 solenoid + 1 HWR per period) and to -15 deg in the β=0.3 Spoke section (1 quadrupole doublet +3 spoke cavities per period). The solenoid field causes x-y phase space mixing with associated emittance growth, especially at low beam energy. The use of alternate sign of the field in subsequent solenoids allowed to cancel most of this mixing every 2nd solenoid, reducing significantly the emittance growth caused by this effect.

Transport of D$^+$ and ^{3}He^{++} beams was less demanding due to the lower space charge forces in comparison with the H$^-$ beam.

The transition between different HWR cryostats includes a drift, which interrupts the lattice regularity and is a potential cause of beam mismatch. Good matching was obtained simply by adjusting the cavity and solenoids fields near transition (usually 4÷6 elements in total). Also the matching between the β=0.09 and the β=0.16 HWR sections was obtained by smooth adjustment of their last and first periods, respectively.

Matching between the 176 MHz HWR and the 352 MHz SPOKE sections required a relatively strong rebunching in the 1st spoke cryostat to accommodate the frequency jump, and a quadrupole triplet before the first cryostat as explained before.

Smooth transport in the Triple Spoke section could be accomplished by matching the beam for constant gradients in cavities and quadrupoles.
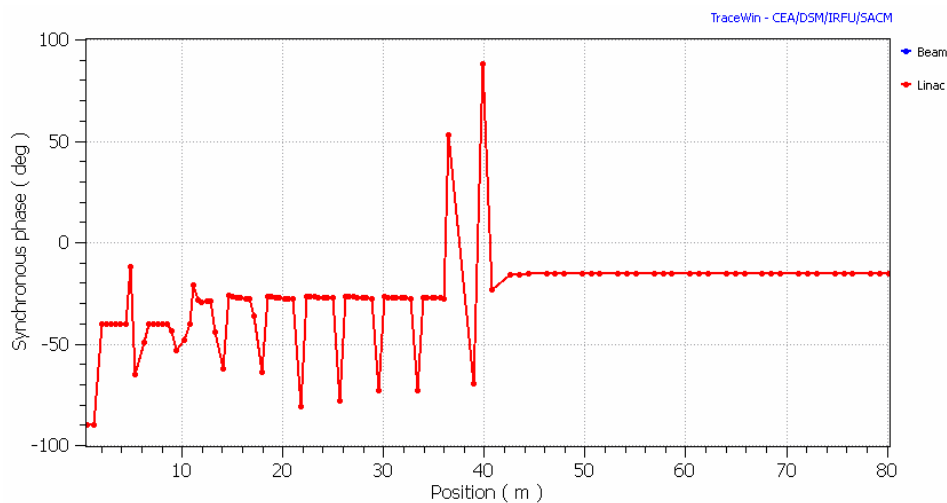
Figure 4.2. H⁻ beam synchronous phase profile in the LMB. The deviation from the nominal phase values are located in cavities used for bunching and matching purposes.

4.2 Multiparticle simulations

Simulations were performed using the beam distribution at the RFQ output (~90000 macroparticles) obtained by the Ion Injector simulation (see deliverable 5-Ion Injector). 1D field maps give an insufficient representation of HWR resonators, and 3D realistic field maps were used for HWR cavities, bunchers and also for solenoids. Field maps of both SARAF and EURISOL type HWR cavities (see chapter 5) were used, with a slightly different adjustment of the beam velocity profiles but with no significant change in the final beam characteristics.

Both 1D and 3D field maps were used for the Triple-Spoke cavities. Differently for the HWR case, for Triple Spoke cavities no visible differences appeared in the simulations results, except for computing time.

4.2.1 MEBT

RIDS 515768	TASK: 7	DATE: 3/2009	
DELIVERABLE: D3-LOW- AND MEDIUM-β LINAC		PAGE 24	

The MEBT was optimized for optimum twiss parameters at the 1st cryostat input with all beams. This section was designed to filter completely the particles transmitted, but not accelerated, in the RFQ before they reach the first cryostat. Most of these particles are overfocused by the quadrupoles and lost in the MEBT; due to their low energy, however, their power deposition is very low. A 5 mm radius diaphragm was put at the end of the MEBT in order to limit the transverse halo at the linac input. The H- beam, which presents the larger space charge defocusing among the possible beams, was studied first. Similar results were eventually obtained for D^+ and $^3He^{++}$.
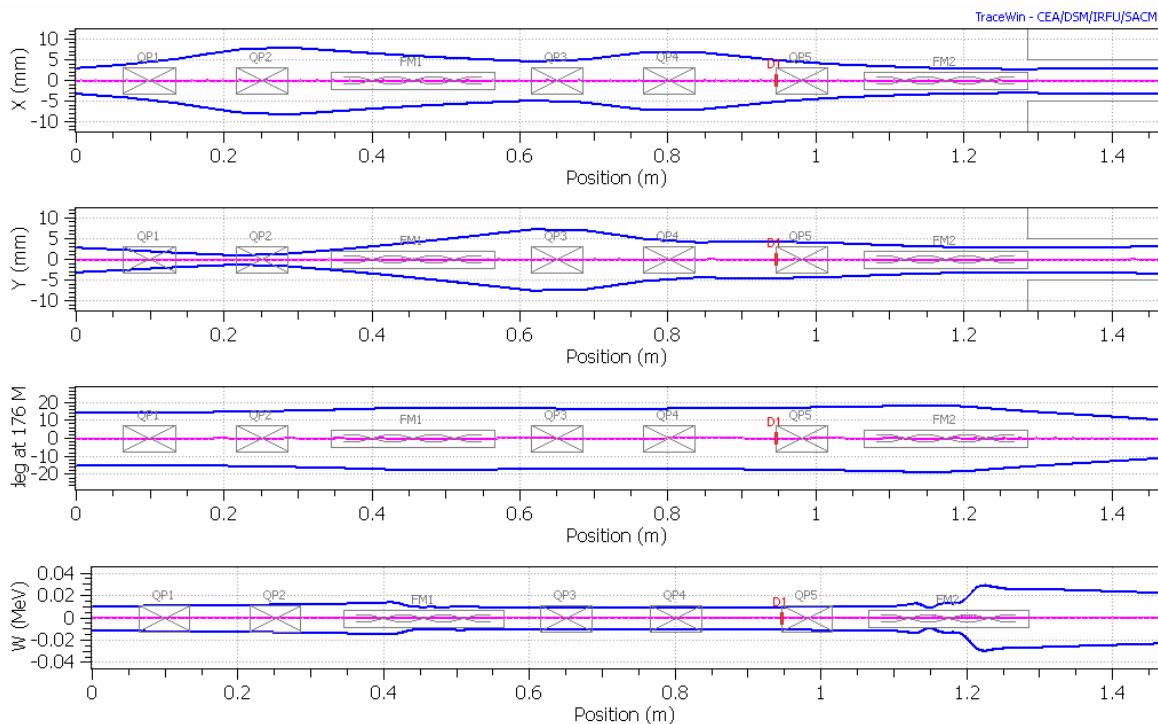
Figure 4.3. H- Beam envelope in the MEBT.
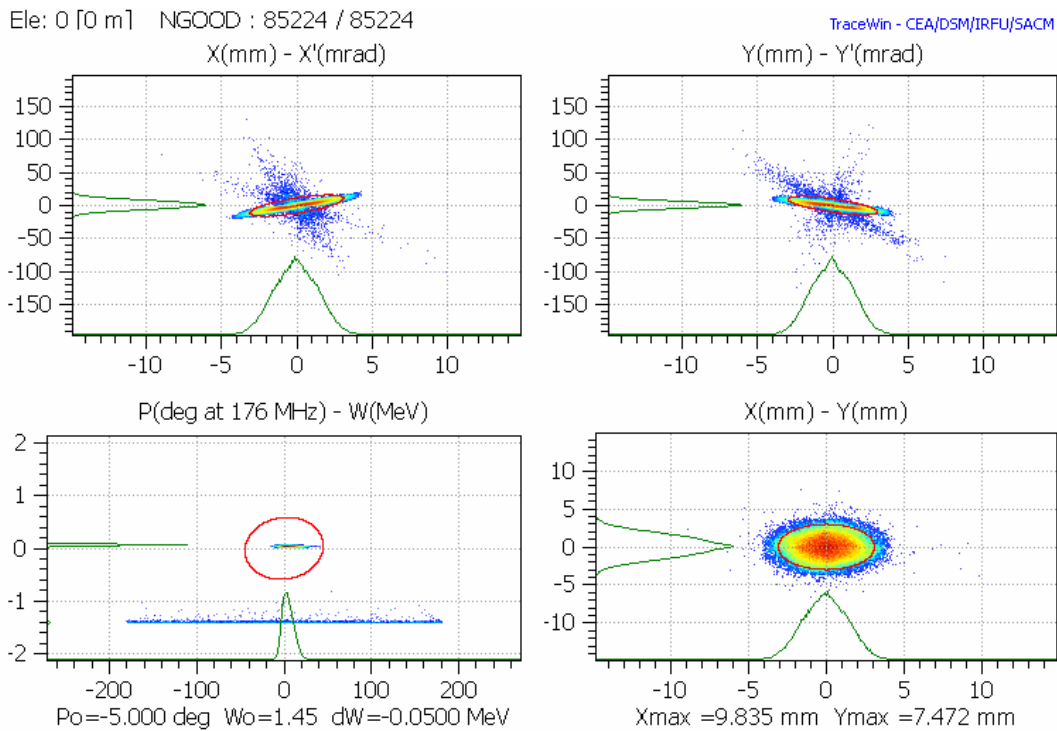
Figure 4.4. H⁻ all-particles phase space distributions from the RFQ. The low energy tail in the phase-energy plot represents the particles transmitted but not accelerated in the RFQ, that appear as irregular rays in the transverse phase space planes.

Steerers can be used in the 1st and 5th quadrupoles to correct input beam misalignment. For this scope, a beam position monitor is needed before the 5th quadrupole and in front of the 1st cryostat. The quarter-wave resonator bunchers (represented with a realistic field distribution calculated with the commercial code CST STUDIO SUITE) give a slight vertical steering to the beam, which is comparable to the effect of a 0.1 mm cavity misalignment, as expected. The effects of this steering appear to be negligible and can be anyhow corrected by an equivalent misalignment in the opposite direction.
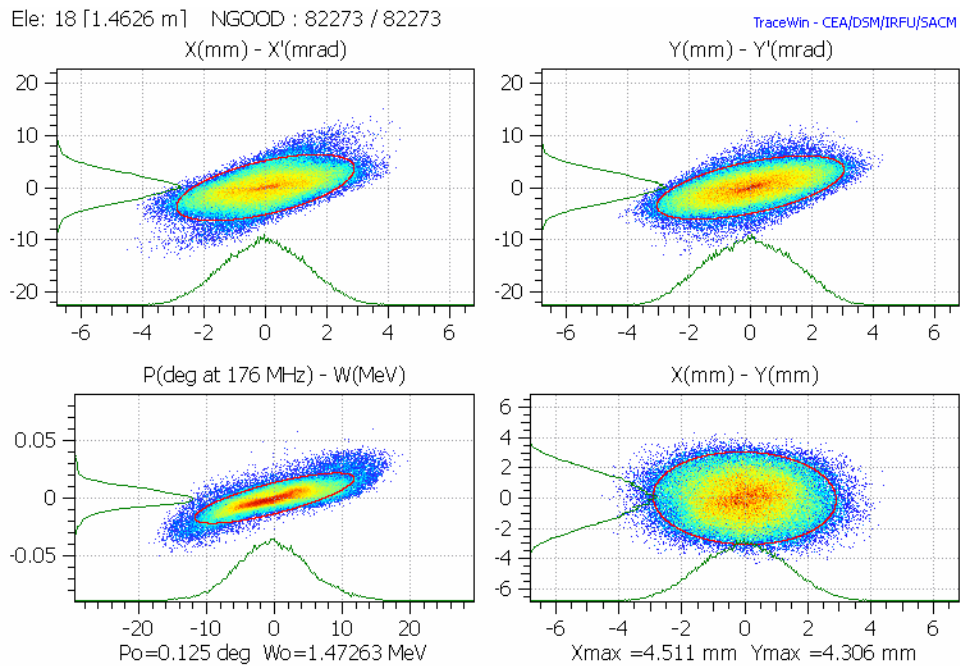
Figure 4.5. H⁻ phase space distributions at the MEBT output (the scale is changed from the previous plots). The low energy tail is completely removed by the MEBT.
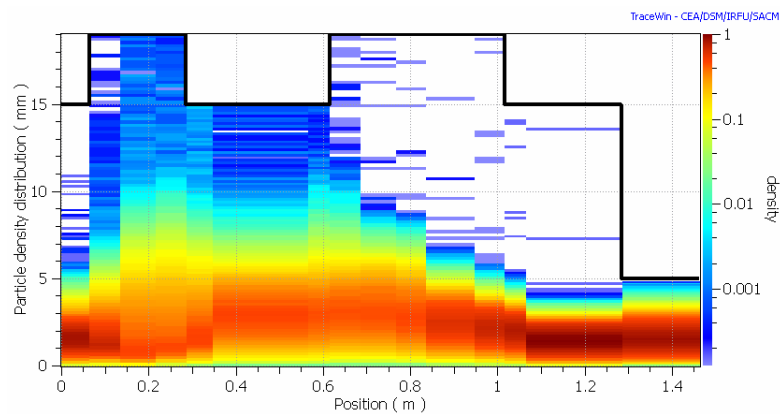

Figure 4.6. H⁻ particle density distribution in the MEBT, showing that most of the low-energy tail is lost in the first half of the MEBT.
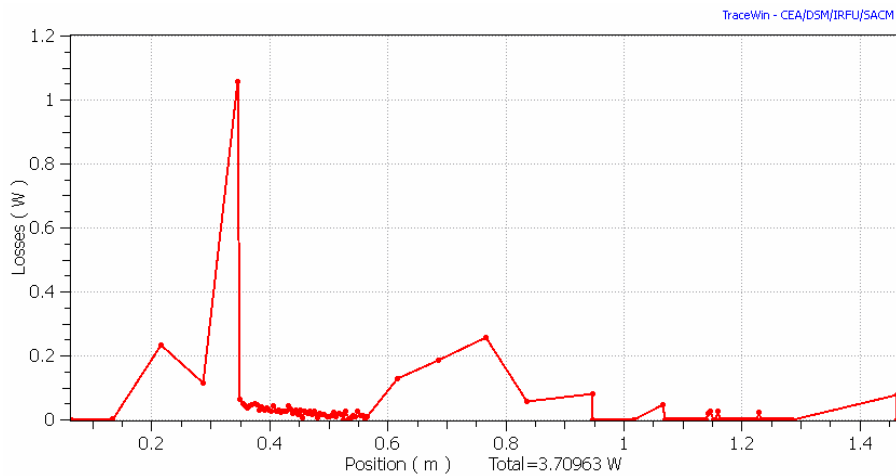
Figure 4.7 Beam power loss distribution along the MEBT for H⁻ beam, caused by the particles transmitted, but not accelerated, in the RFQ.

4.2.2 SC linac

The SC linac includes the β=0.09, the β=0.16, the matching and the β=0.3 sections. The HWR modules consist of one cryostat and the following drift space; the β=0.3 modules consist of a quadrupole doublet, one cryostat and the following drift space. One more quadrupole is added to the first β=0.3 module doublet to improve matching between different sections.

The first part of the HWR section represents a critical part of the linac. The large rf defocusing, caused by the large energy gain fraction per resonator, and the space charge forces which are still significant at the energy of 1.5 MeV/q for the 5 mA beams, are a potential source of emittance growth. To limit the longitudinal phase advance and rf defocusing, acceleration was limited to $\Delta W/W \sim 0.35$ in the 1st cryostat.

To correct possible aligment errors, 2 beam position monitors and 2 steerers per cryomodule can be used in the HWR section and 1 BPM and 1 steerer per module in the SPOKE section (see table 4.2).

RIDS 515768	**TASK: 7**	**DATE: 3/2009**	
DELIVERABLE:	**D3-LOW- AND MEDIUM-β LINAC**	**PAGE** 28	

Table 4.2. SC linac beam correction system summary.

	MEBT	β=0.09 cryostats	β=0.16 cryostats	β=0.3 cryostats
1st BPM location	Before 5th quad	after 5th solenoid	after 3rd solenoid	Between quads
2nd BPM location	MEBT end	after each cryostat	after each cryostat	-
BPM resolution mm	0.1	0.1	0.1	0.1
Steerer 1 location	1st quadrupole	1st solenoid	1st solenoid	after doublet
Steerer 2 location	5th quadrupole	6th solenoid	3rd solenoid	-

4.2.2.1 Simulation without errors

The beam transport along MEBT and SC Linac was simulated using the RFQ output beam distributions for H$^-$, D$^+$, ^{3}He^{++} with about 90000 macroparticles (see Deliverable 5 – Ion Injector), showing lossless transport with moderate emittance growth along the all LMB linac and good correspondence with the final specifications for all beams (Table 4.3).

Table 4.3. Summary of the simulations results without errors

	H$^-$	D$^+$	^{3}He^{++}
Beam current mA	5	5	0.1
Output energy (MeV)	130	172	312
Input emittance ε_x, ε_y, ε_z $\pi\cdot$mm$\cdot$mrad	0.17, 0.17, 16	0.15, 0.15, 0.19	0.14, 0.14, 0.34
Output emittance ε_x, ε_y, ε_z $\pi\cdot$mm$\cdot$mrad	0.20, 0.19, 0.19	0.16, 0.16, 0.19	0.15, 0.15, 0.35
Transmission (after MEBT) %	100	100	100

H- beam. The H$^-$ case is the more demanding one, presenting the larger space charge problems. However, simumulations could allow acceleration with good beam quality. The aperture to rms beam ratio after the MEBT diaphragm could be kept above 7 up to cavity n. 20 (3rd cryostat), and above 10 all along the rest of the linac. Emittance growth and halo are within the design goals.

D$^+$ beam. The results obtained with the D$^+$ beam are similar to the H$^-$ ones, with the exception of a slight halo formation in the longitudinal plane (see fig. 4.13). The D$^+$ beam, however, is accelerated only in the first part of the high-β linac and then debunched and transported without acceleration to

the target area (see Deliverables D4 and D6), making longitudinal halos less critical for beam losses in comparison with the H⁻ beam case.

³He⁺⁺ beam. This beam is characterised by low space charge and by inhomogeneous distribution of the particle delivered by the RFQ in the longitudinal phase space (fig. 4.17). This results in a large longitudinal input emittance, which can be anyhow preserved during acceleration (fig. 4.19).
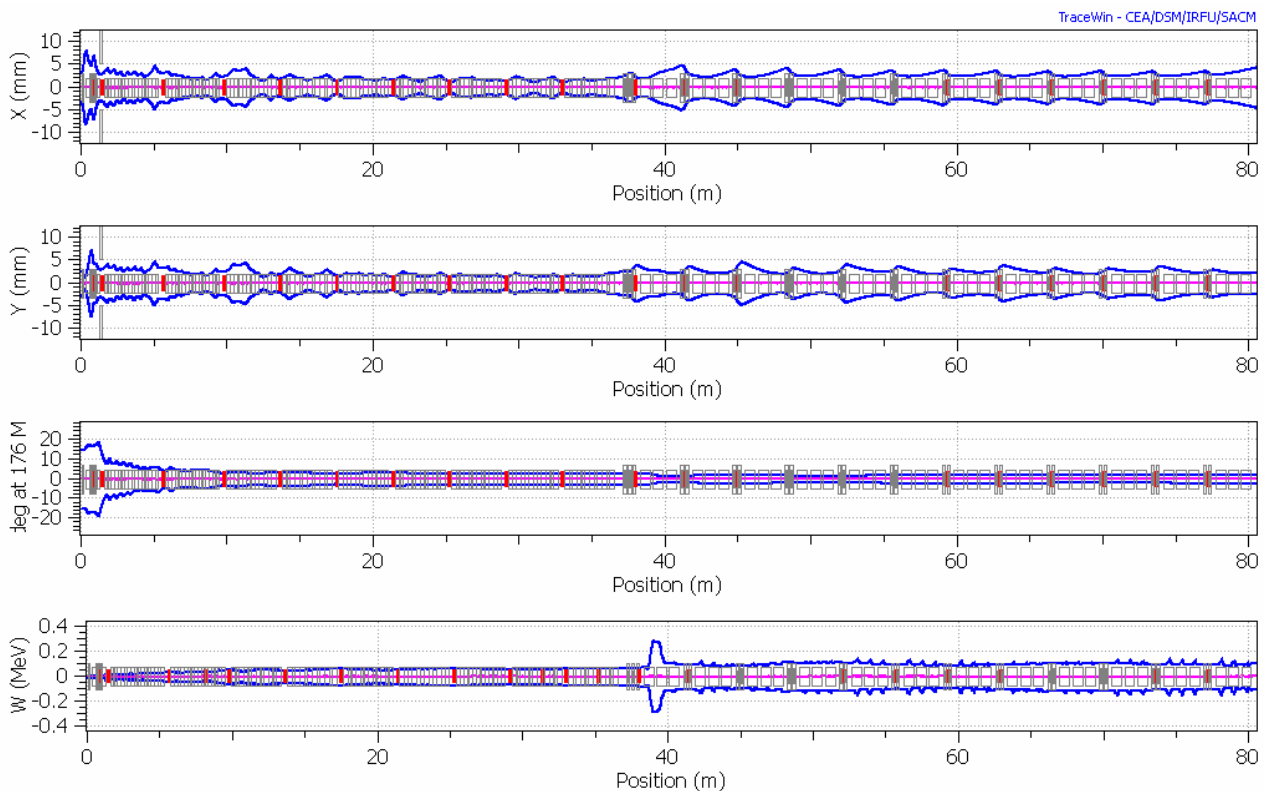

Figure 4.8. 2 rms envelope plot for H⁻.
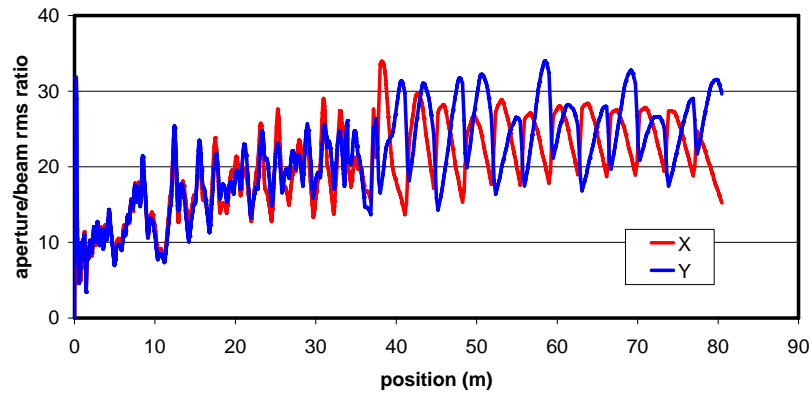
Figure 4.9. Beam line aperture to rms beam size along the MEBT and the linac, for H⁻. The minimum is located at the MEBT diaphragm.

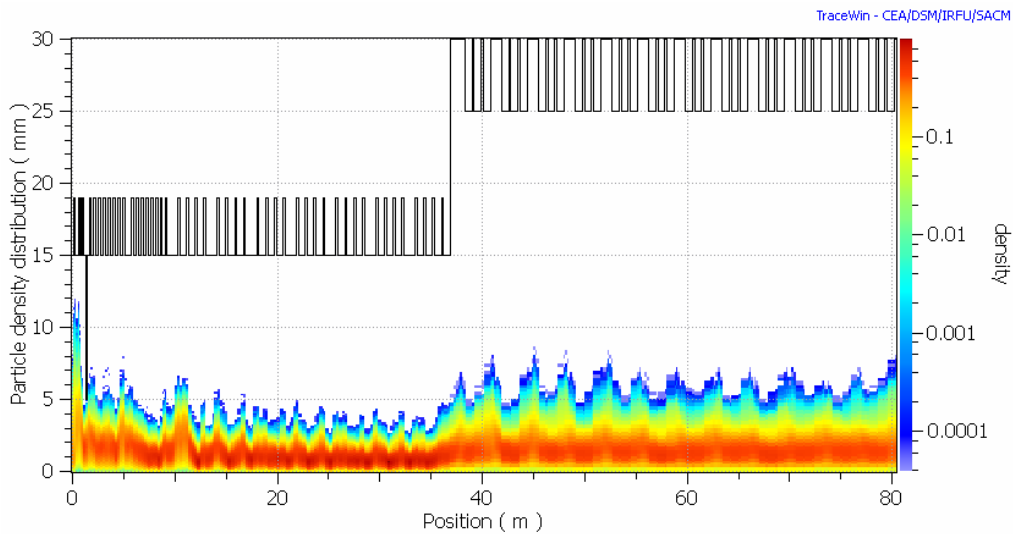Figure 4.10 Left: Particle density distribution along the linac for H⁻. The black line represents the beam pipe aperture.
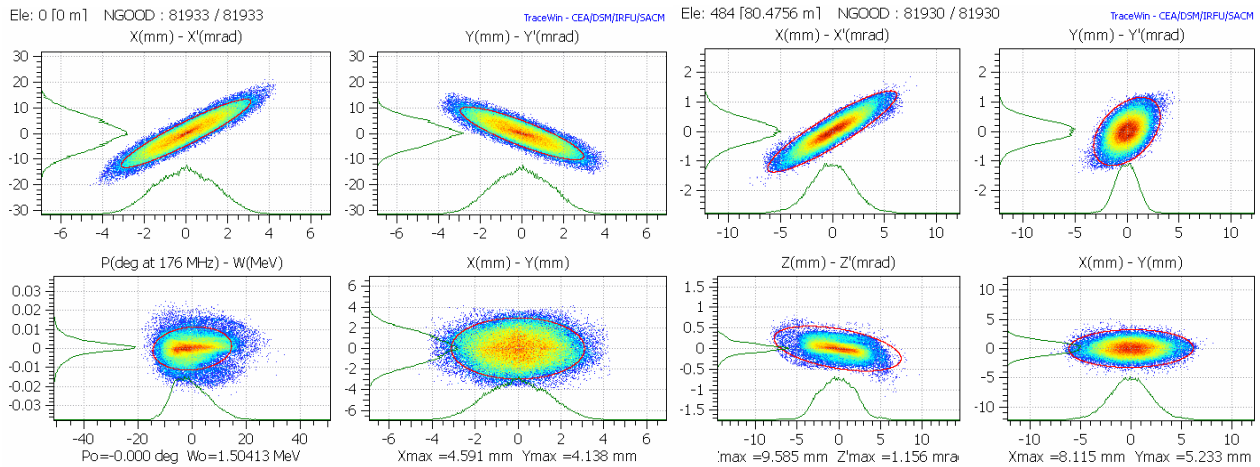
Figure 4.11. Left: H⁻ phase space at the linac input (left) and output. 99% emittance ellipses in red. The phase space distributions from the RFQ includes only the accelerated particles (the low energy tail which is lost in the MEBT is not represented in the graphs).
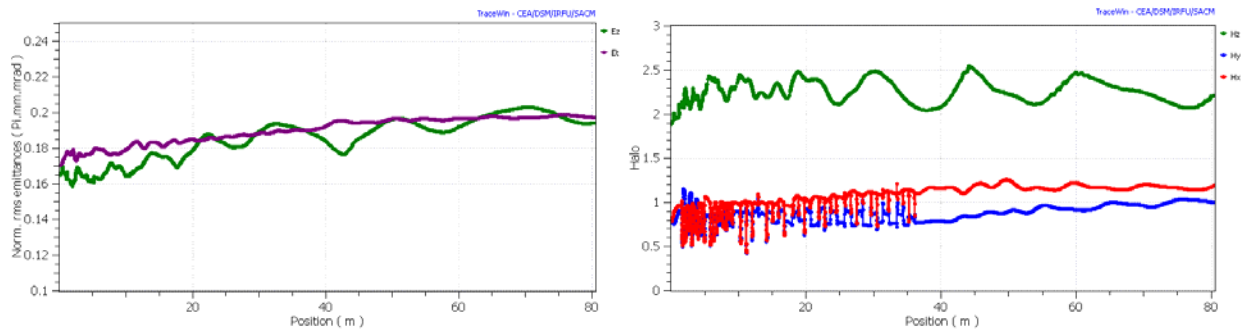

Figure 4.12. Normalized rms H⁻ beam emittance evolution (left) and halo parameter along the linac.
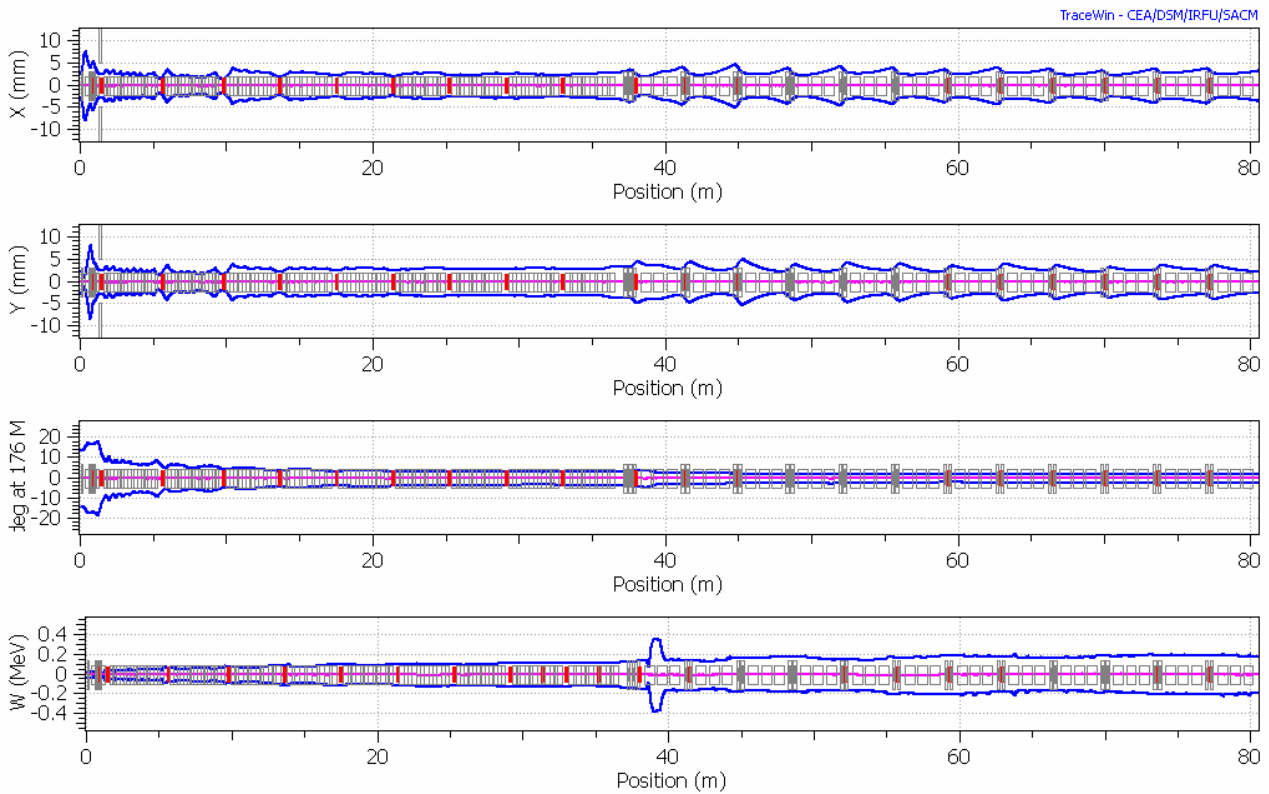
Figure 4.13. 2 rms envelope for D^+.
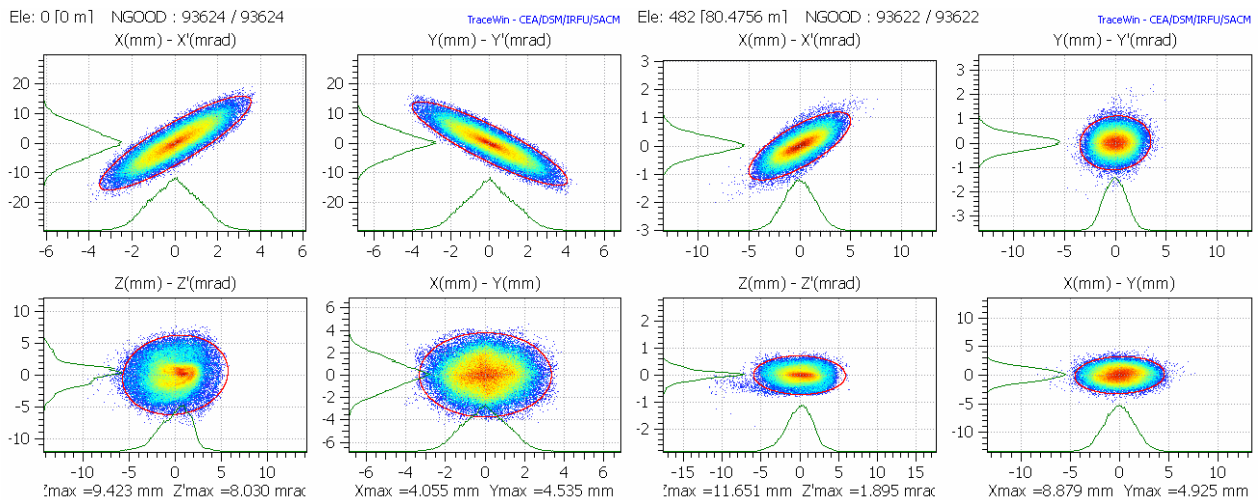

Figure 4.14. D^+ phase space at the linac input (left) and output. 99% emittance ellipse in red.

RIDS 515768	TASK: 7	DATE: 3/2009	
DELIVERABLE: D3-LOW- AND MEDIUM-β LINAC		PAGE 34	

Figure 4.15. Particle density distribution along the linac for D$^+$.
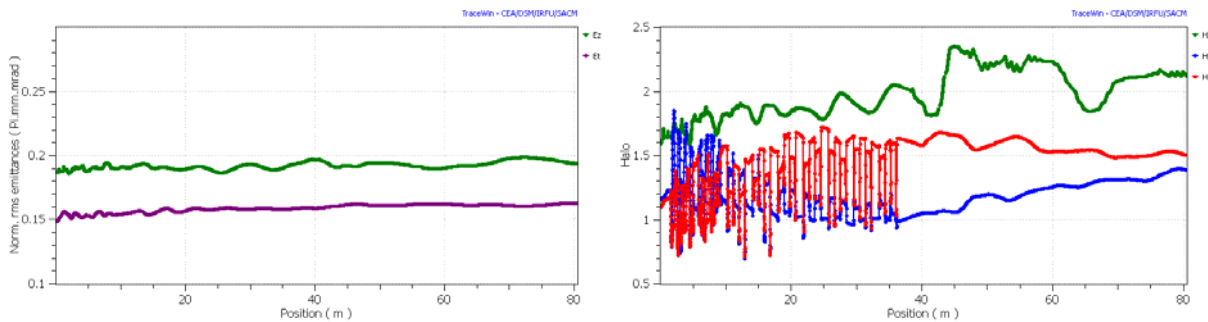
Figure 4.16. Emittance evolution (left) and halo parameter along the linac for D$^+$
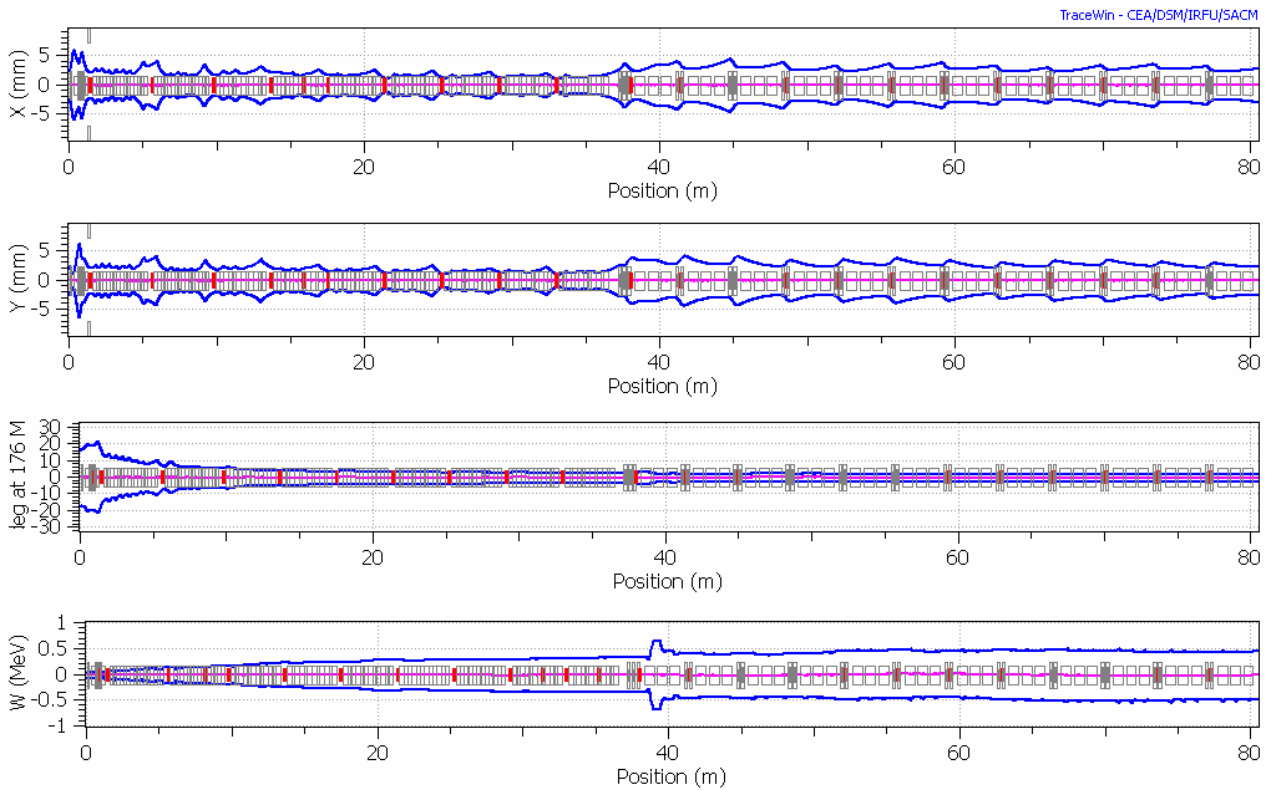
Figure 4.17. 2 rms envelope for ^{3}He^{++}.
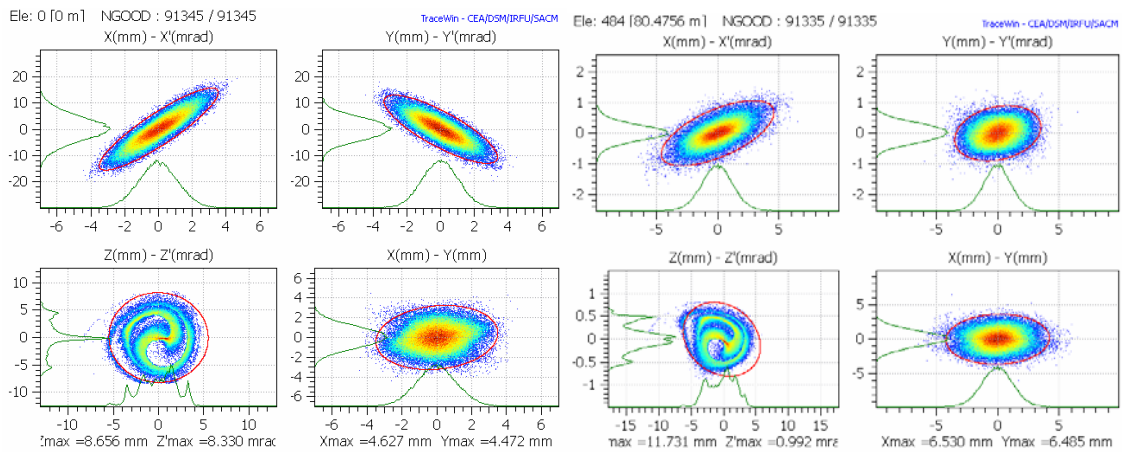
Figure 4.18. ^{3}He^{++} phase space at the linac input (left) and output. 99% emittance ellipses in red.
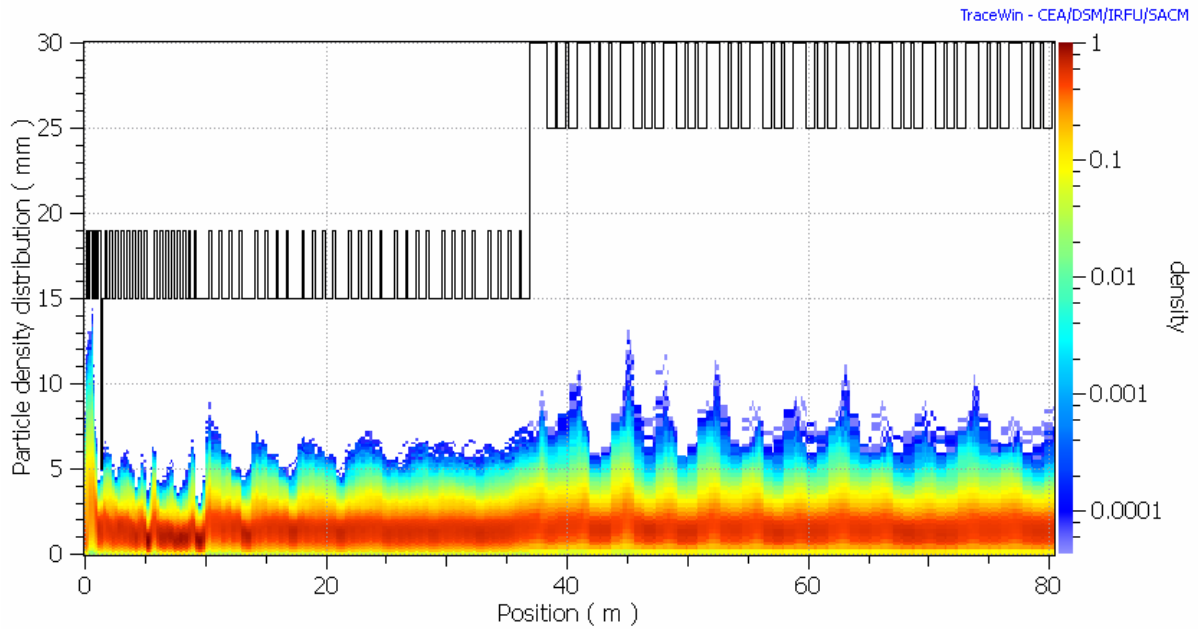
Figure 4.19. Particle density distribution along the linac for ^{3}He^{++}.
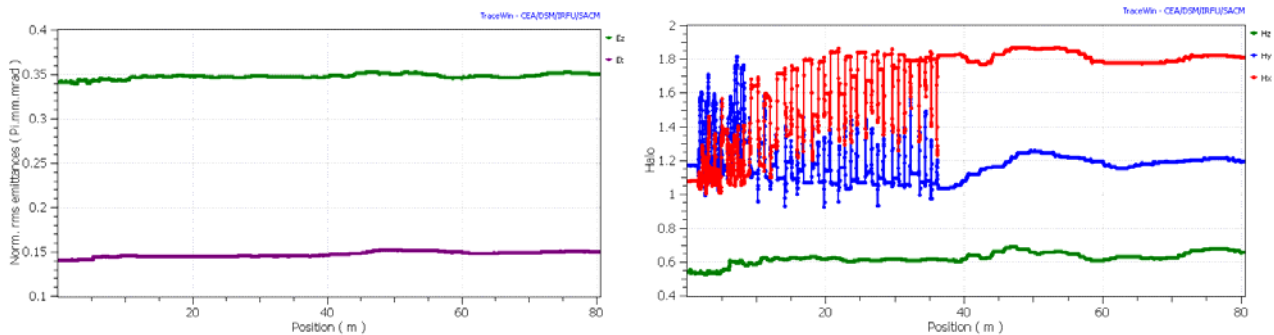
Figure 4.20. Emittance evolution (left) and halo parameter along the linac for ^{3}He^{++}.

4.3 Simulation with errors

In the simulation without errors with ~10^5 macroparticles no beam losses have been found, except for the low energy particles lost in the MEBT. In order to verify the possibility to operate the linac in the presence of realistic errors (misalignment, field amplitude and phase, etc.- see table 4.4), a preliminary simulation with errors has been done. Acceptable values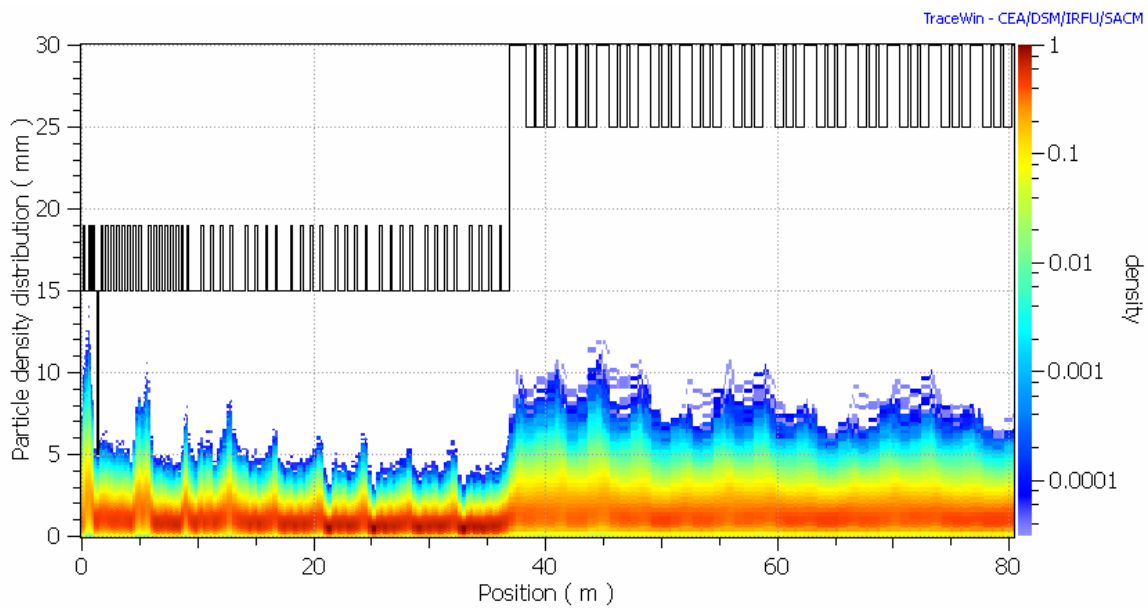 for these errors were preliminarly assessed, and used for the final error study and beam loss calculations with large statistics, reported in Deliverable D7-Beam loss calculations. Minimum steerers requirements were also evaluated in this study.

We have chosen a set of maximum error values realistically achievable with the present technology. The input beam errors have been set in agreement with the injector output beam ones, estimated in the simulations of that linac section (see Deliverable D5-Ion Injector).

We tested the linac with 100 different simulation runs, each one with 5000 particles and with a different set of errors randomly distributed in the allowed interval, for a total of 500000 macroparticles. The transverse errors were corrected, as possible, by means of steerers and BPMs with the specifications described in Table 4.2. No correction in the longitudinal phase space was performed. We have then determined the statistical errors induced in the output beam by these errors, and used this information to optimize the correction system. The goal was to find an efficient correction system with a minimum number of steerers and diagnostics elements.

The results for the final configuration described in the report are shown in Table 4.5 and in the following graphs. However, the final assessmentof the the correction system effectiveness in the presence of the nominal errors was performed with very large statistics in the error study of the whole linac, which results can be found in Deliverable D7-Beam loss calculations.

Table 4.4. Maximum input errors introduced in the LMB linac.

type	error	unit	MEBT	HWR	SPOKE
Input beam					
static+dynamic	displacement X	mm	0.1	-	-
	displacement Y	mm	0.1	-	-
	displacement X'	mrad	0.1	-	-
	displacement Y'	mrad	0.1	-	-
	displacement phase	deg	0.1	-	-
	displacement Energy	MeV	0.001	-	-
	ε_x increase	%	10	-	-
	ε_y increase	%	10	-	-
	ε_z increase	%	10	-	-
	mismatch XX'	%	10	-	-
	mismatch YY'	%	10	-	-
	mismatch ZZ'	%	10	-	-
static	beam current	mA	0.5	-	-
dynamic	beam current	mA	0.1	-	-
Quadrupole magnets					
static	displacement X	mm	0.1	-	0.1
	displacement Y	mm	0.1	-	0.1
	angle ϕ_x	deg	0.16	-	0.06
	angle ϕ_y	deg	0.16	-	0.06
	angle ϕ_z	deg	0.03	-	0.03
	gradient	%	0.5	-	0.5
	displacement Z	mm	1	-	1
Cavities					
Static	displacement X	mm	0.5	0.5	0.5
	displacement Y	mm	0.5	0.5	0.5
	angle ϕ_x	deg	0.25	0.25	0.25
	angle ϕ_y	deg	0.25	0.25	0.25
	phase error	deg	2	1	1
	Amplitude error	%	1	1	1
	displacement Z	mm	1	1	1
dynamic	phase error	deg	0.1	0.1	0.1
	Amplitude error	%	0.1	0.1	0.1
SC solenoid magnets					
static	displacement X	mm	-	0.25	-
	displacement Y	mm	-	0.25	-
	angle ϕ_x	deg	-	0.125	-
	angle ϕ_y	deg	-	0.125	-
	angle ϕ_z	deg	-	1	-
	gradient	%	-	1	
	displacement Z	mm	-	1	

Table 4.5. LMB linac output beams statistic errors estimate resulting from the preliminary simulation with ~500000 macroparticles, in the presence of random errors in the input beams and in the linac parameters, corrected with steerers and BPMs.

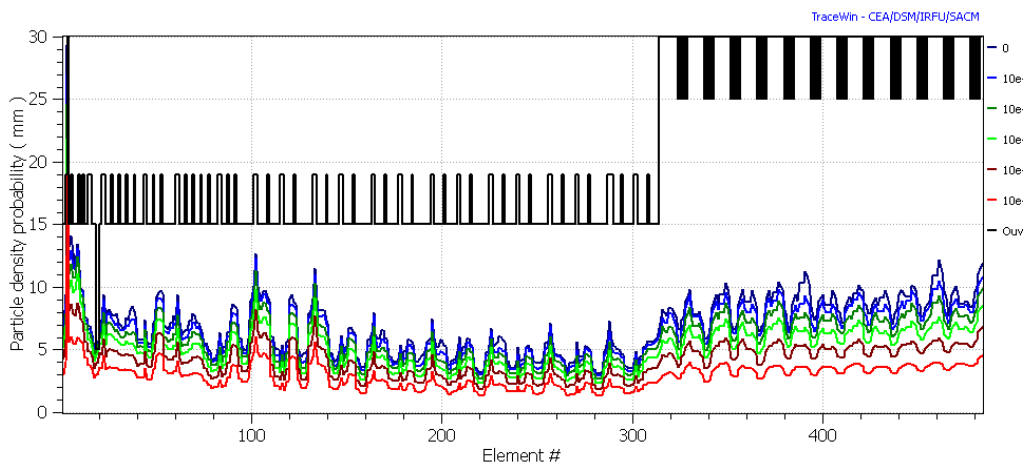| Rms error type	symbol	unit	Output beam error (rms)		
			H^-	D^+	$^3He^{++}$
Position x	δx	mm	1.4	1.2	0.12
Position y	δy	mm	1.2	1.2	0.11
Phase	$\delta\phi$	deg	1.5	1.2	0.1
Angle x	$\delta x'$	mrad	0.3	0.3	0.01
Angle y	$\delta y'$	mrad	0.4	0. 4	0.01
Energy	δE	keV/u	144	72	8
Emittance growth x	$\delta\varepsilon_x$	%	6	6	3
Emittance growth y	$\delta\varepsilon_y$	%	3	1	0.6
Emittance growth z	$\delta\varepsilon_z$	%	19	25	1.6

Figure 4.21. H^- particle density probability along the Low- and Medium-β linac, simulated with 500000 macroparticles. Sum of 100 runs of 5000 macro particles with different sets of random errors.

5 Linac technology

In this chapter the main components of the linac are described and the technological choices discussed in order to assess their availability. Components which are neither available on the market nor in operation in other facilities, and components which have been especially designd or developed for EURISOL will be described in some detail.

5.1 MEBT

The main specifications of the MEBT components are listed in par. 3.2. In addition to the MEBT layout, the only component that required a special design for the EURISOL driver is the buncher resonator. All other components are in operation at SARAF.

5.1.1 Buncher resonators

The MEBT bunchers are Quarter-Wave Resonators (QWRs) working at 176 MHz. Their design have some similarities to the one of the INFN-Legnaro 80 MHz high energy bunchers, working at similar voltage, β and rf power [19], rescaled and re-optimized for operation at the EURISOL frequency. For this combination of frequency and beam velocity ($\beta=0.056$), the usual spacing of $\beta\lambda/2$ between the two accelerating gaps operated in π-mode is 47 mm. With 15 mm gap and 30 mm aperture diameter, the resulting transit time factor has an acceptable value of $T(\beta_0)\sim0.76$. The calculated rf power requirements, including a 20% safety margin in the field, are about 4 kW for the first cavity and 14 kW for the second one.

Quarter-wave resonators, when operated at optimum velocity and -90° synchronous phase, are potentially dangerous for beam steering caused by transverse magnetic field typically present on the QWR beam axis (fig. 5.3) [18]. In the EURISOL MEBT case, however, the required gradient is rather low, and steering compensation can be easily accomplished by a slight displacement of the

RIDS 515768	TASK: 7	DATE: 3/2009	
DELIVERABLE: D3-LOW- AND MEDIUM-β LINAC		PAGE 41	

resonator beam axis (~ 0.1 mm, comparable to the alignment precision) and by the use of the MEBT vertical steerers.
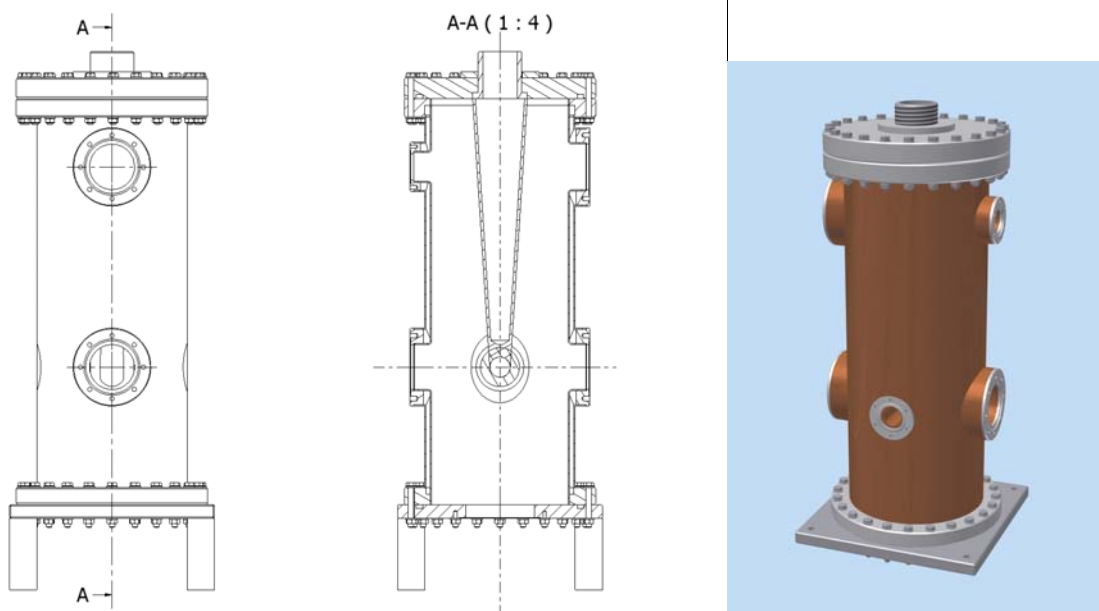

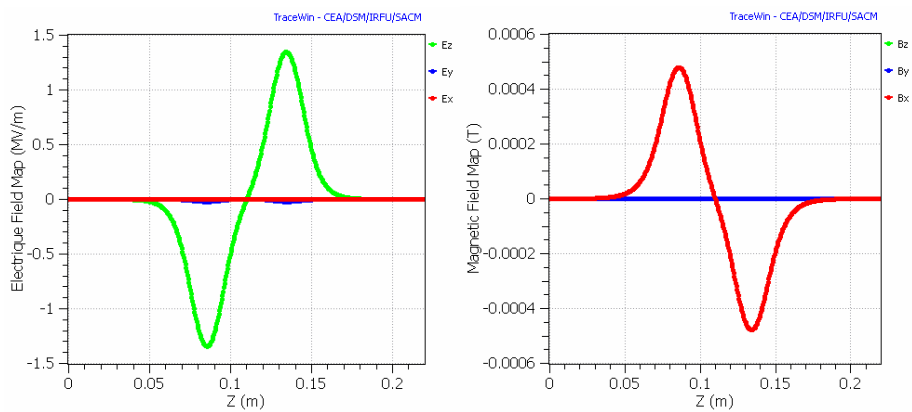Figure 5.1. Sketch and 3D view of the MEBT buncher resonator model.

Figure 5.2. On-axis electric and magnetic field distributions of the MEBT bunchers.

Table 5.1. Main parameters of the MEBT buncher cavities.

Frequency	MHz	f	176
Optimum v/c		β_0	0.056
Transit-time factor		$T(\beta_0)$	0.76
Max accelerating field	MV/m	E_a	1
Max voltage on the gap	kV	V_g	130
Quality factor		Q_o	$\sim 10^4$
RF power at maximum E_a	kW	P	9
Shunt impedance $E_a^2/(P/l)$	MΩ/m	$R'sh$	22
Norm. shunt impedance	kΩ/m	$R'sh/Q_o$	2.2
Acceleration length	m	l	0.2
Physical length flange to flange	m	h	0.22
Aperture diameter	mm	a	30

5.2 Low-β linac

5.2.1 Choice of the accelerator technology

The EURISOL specifications impose a superconducting linac, ideally suited for cw operation due to its low rf losses. The technological choice of superconducting Half-Wave Resonators (HWRs) for the low-β linac section was motivated by the following considerations:

- Cavities with large velocity acceptance are required in order to accelerate efficiently beams with different A/q (H$^-$, D$^+$, 3He^{++}) up to ~60 MeV/u. 2-gap cavities are the ideal choice.

- Many superconducting low-β linacs for heavy ions have been constructed and operated in cw mode during the last two decades. They are all of the ISCL (Independently-phased Superconducting Cavity Linac) type, consisting of short (2÷4 gap), low frequency (48÷162 MHz) accelerating cavities. This scheme fits rather well the EURISOL driver low-β linac.

- In the existing machines, the most used resonator type is by far QWR (Quarter-wave resonator), preferred for its relatively low cost, easy mechanical construction and high performance at low-

β. The only significant drawback of this structure is the asymmetry of its shape that can cause beam steering if cavities are operated at high gradient. This can be usually compensated, although never completely, with different techniques. However, in 176 MHz QWRs at high accelerating field the residual steering can create significant emittance growth and losses in high intensity proton beams.

- Half-wave resonators (HWRs) are very similar to QWRs (an HWR can be considered as made of two QWRs joined together at the high voltage side) but their intrinsic symmerty cancels the QWR steering effect completely. This makes HWRs suitable for high current applications with low-β beams, keeping most of the QWR virtues but not their main drawback.

Table 5.2. Worldwide low-β superconducting ion linacs of the ISCL type.

Laboratory	location	Cavity type	status
ANL	Chicago, USA	split-ring and QWR	In operation
INFN-LNL	Padova, Italy	QWR	In operation
TRIUMF	Vancouver, Canada	QWR	In operation
SUNY	Stony Brook, USA	QWR	In operation
JAERI	Ibaraki, Japan	QWR	In operation
IUAC	New Delhi , India	QWR	In operation
ANU	Canberra, Australia	Split ring	In operation
UW	Washington	QWR	dismissed
CEA	Saclay, France	Helix	dismissed
Weizmann Institute	Rehovot, Israel	QWR	dismissed
SOREQ	Yavne, Israel	HWR	Under commissioning
GANIL	Caen, France	QWR	Under construction
IFMIF-EVEDA	Rokkasho, Japan	HWR	Under construction

Other laboratories, although not hosting yet a low-β ISCL, have done extensive studies and cavity prototyping for low-β superconducting linacs,:

1. IPN Orsay (QWR, Spoke)

2. CEA Saclay (QWR, HWR)

3. Michigan State University (USA, QWR and HWR)

4. CIAE Beijing (China, QWR)

5. Forschungszentrum Juelich (Germany, HWR and Spoke)

6. University of Frankfurt (Germany, CH)

7. Los Alamos National Laboratory (USA, Spoke)

8. FERMILAB (USA, Spoke)

The operational experience on Low-β ISCLs is rather wide. The cavity gradient, the voltage and the phase stability, as well as the reliability of the cryostat tecnology, have been widely demonstrated. The state of the art for reliable peak fields in operation is E_p=35 MV/m and B_p=70 mT with double wall, bulk Niobium QWRs in common vacuum cryostats [22].

Concerning reliability, the oldest of these accelerators, the superconducting linac ATLAS at ANL (USA), has accumulated more than two decades of operation. The main source of failure of existing low-β ISCLs is the cryogenic system, when it is made of only one cold box. This is not the case of EURISOL, which will make use of a large cryogenic system feeding the all, 300 m long, superconducting driver linac.

The use of a low-β ISCL with high beam loading can be pursued by a proper rf feeding system for high rf power. This can be obtained by means of the rf coupler and rf power sources technology developed and currently used in other high current superconducting accelerators (e.g. SARAF) and especially optimized for EURISOL in the Task 8 framework.

RIDS 515768 TASK: 7	DATE: 3/2009	
DELIVERABLE: D3-LOW- AND MEDIUM-β LINAC	PAGE 45	

It should be noted that the participants and contributors to the EURISOL accelerator tasks are among the most advanced laboratories in the field of low-β superconducting resonators.

5.2.2 Half-Wave resonators

Two types of HWR cavities, with β = 0.09 and β = 0.16, are required for acceleration up to ~60 MeV/u. HWRs with similar characteristics have been recently developed and built for the SARAF project [10] which is now under commissioning, and could be used for EURISOL. However, their mechanical design make them very sensitive to mechanical disturbances and difficult to operate; this characteristics put severe requirements to the cryogenic system stability and to the mechnical tuner capabilities.

HWRs in the same range of frequency and beam velocity are under development for the 125 mA deuteron linac of the IFMIF project [4], and might also be utilized in EURISOL after downgrading the large rf coupler for operation at 5 mA.

Half-wave resonators have been specifically designed for the EURISOL driver in the Task 8 framework [9]. They are double-wall structures with good mechanical stability against Helium pressure variation and Lorentz force, and their design allows easy installation in different kinds of cryostats both with common and separate vacuum.

Mechanical design - The EURISOL HWRs (Fig. 5.3) have been designed paying particular attention to mechanical stability. These cavities are characterized by a double-wall coaxial structure terminated by thick plates, with integrated helium vessel [9]. This makes them very compact and stiff, even if the resonators are made in a large part of 2 mm thick Nb sheets. The cavities are of 2 types, ''flattened'' and ''cylindrical,'' named after their inner conductors' shapes, with maximum physical lengths along the beam axis of 232 and 286 mm, respectively. The beam port aperture diameter is 30 mm, as specified by the beam dynamics calculations (a significant increase of this value, if needed, would require increasing of the resonator's size).

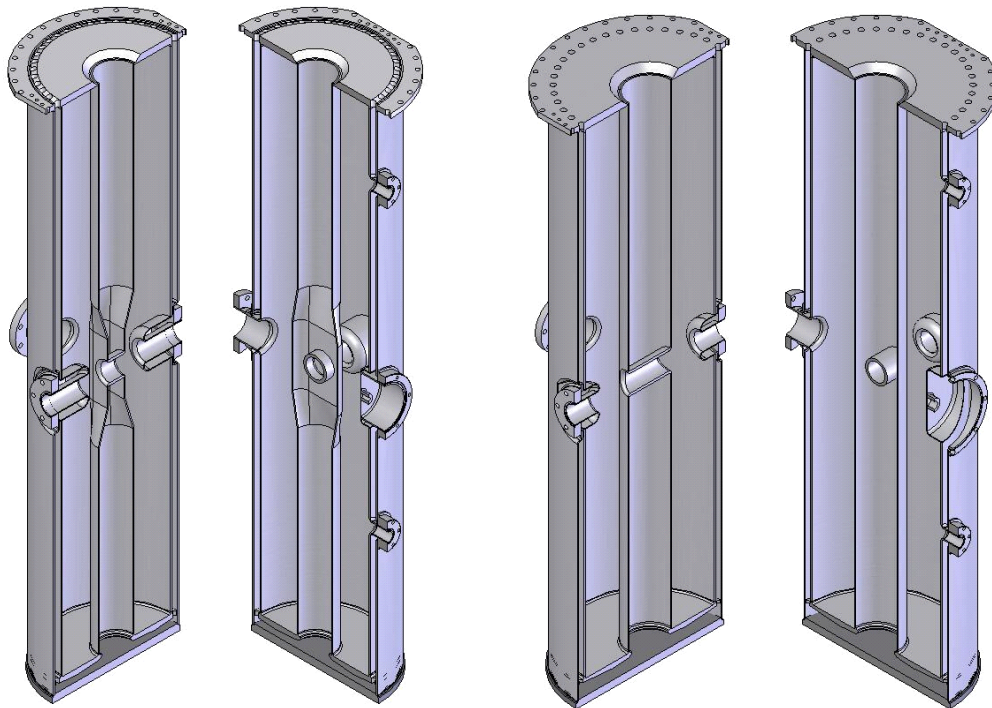| RIDS 515768	TASK: 7	DATE: 3/2009	
DELIVERABLE: D3-LOW- AND MEDIUM-β LINAC		PAGE 46	

Figure 5.3. Sketch of the EURISOL 176 MHz, half-wave resonators, cut in two perpendicular planes. Left: $\beta_0 = 0.09$ HWR; Right: $\beta_0 = 0.16$

A $1^5/_8$ -inch port for a coaxial rf coupler is located at the resonator's equator, at one side of the outer conductor. According to the rf power requirements, a larger coupling port up to $3^1/_8$ -inch could be implemented in the same design without major difficulties. Two more, 16 mm ports are available for rf probes. The rf port's position was chosen also in order to facilitate chemical polishing. These resonators are designed for cryostats which have in common the rf-beam volume and the one required for thermal isolation, included in only one vacuum system (common vacuum cryostats); all ports, however, are equipped with flanges that allow for use in cryostats with vacuum separation.

A tuning cup (Fig. 5.4) is welded to the outer conductor, at the opposite side from the coupler. To improve the frequency stability against pressure fluctuations, the membrane which provides tuning is cooled by thermal conduction and is not exposed to liquid helium. This tuner is decoupled from the beam ports and its force requirements are rather modest. The beam ports and the rf ports flanges are made of NbTi, as well as the outer flange of the tuning cup where a tuning mechanism can be easily mounted. A drawback of this system is the limited tuning range (below 50 kHz at present) that requires a very precise cavity construction. The double-wall cavity has its own Helium vessel, connected to the helium reservoir through a conflat flange that makes its assembly in the cryostat particularly easy.

Figure 5.4. Detail of the tuning cup before welding to the resonator.

Electromagnetic design - The resonators rf parameters, calculated with the HFSS and CST codes, are shown in Table 5.3. The E_p/E_a and B_p/E_a values are not far from the ones of QWRs working at similar frequency. The design gradient in operation at 4.2 K was set at 4.7 and 5.2 MV/m for the $\beta=0.09$ and $\beta=0.16$ units, respectively, with 10 W rf power. This gives 0.9 and 1.34 MeV/q energy gain, respectively. The specified maximum surface fields in operation are $B_p \sim 70$ mT and $E_p \sim 30$ MV/m, achieved according to the available statistics in cavities of similar frequency and β [22].

Figure 5.5. HWR mechanical tuner

Although the HWR symmetry prevents vertical beam steering, the effects on the beam of the electromagnetic field distribution have been

RIDS 515768	TASK: 7	DATE: 3/2009	
DELIVERABLE: D3-LOW- AND MEDIUM-β LINAC		PAGE 48	

calculated to evaluate the effect of the side tuner, that could cause horizontal steering, and the one of the quadrupolar symmetry that could cause unwanted quadrupolar focusing-defocusing. Similarly to rf defocusing, these effects are a function of the particle velocity and phase. We found that the side tuner steering, at operation ϕ, β, and E_a, is weak and negligible compared to rf defocusing [9].

Table 5.3. Calculated parameters of the double-wall Half-wave resonators designed for the EURISOL driver.

Resonator type	HWR1	HWR2	units
β	0.085	0.155	
U/E_a^2	0.134	0.173	$J/(MV/m)^2$
B_p/E_a	12.4	11.7	$mT/(MV/m)$
E_p/E_a	5.8	4.2	
R'_{sh}/Q_0 $(E_a^2 L /(Q_0 P))$	1215	1181	Ω/m
$R_s \times Q_0$	31.9	38.2	Ω
Active length L	180	224	mm
Maximum Length L_{re}	232	286	mm
Aperture diameter a	30	30	mm
Design E_a	5	6	MV/m
He Pressure detuning	1	3.7	Hz/mbar
Lorentz force detuning	-3.6	-1	$Hz/(MV/m)^2$
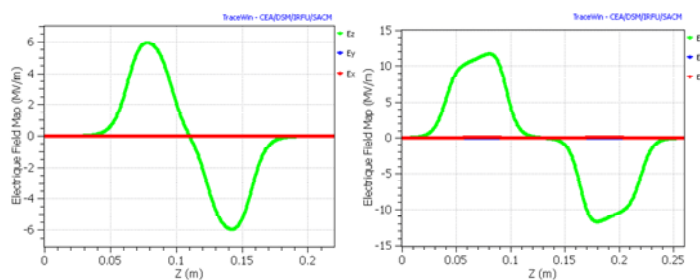
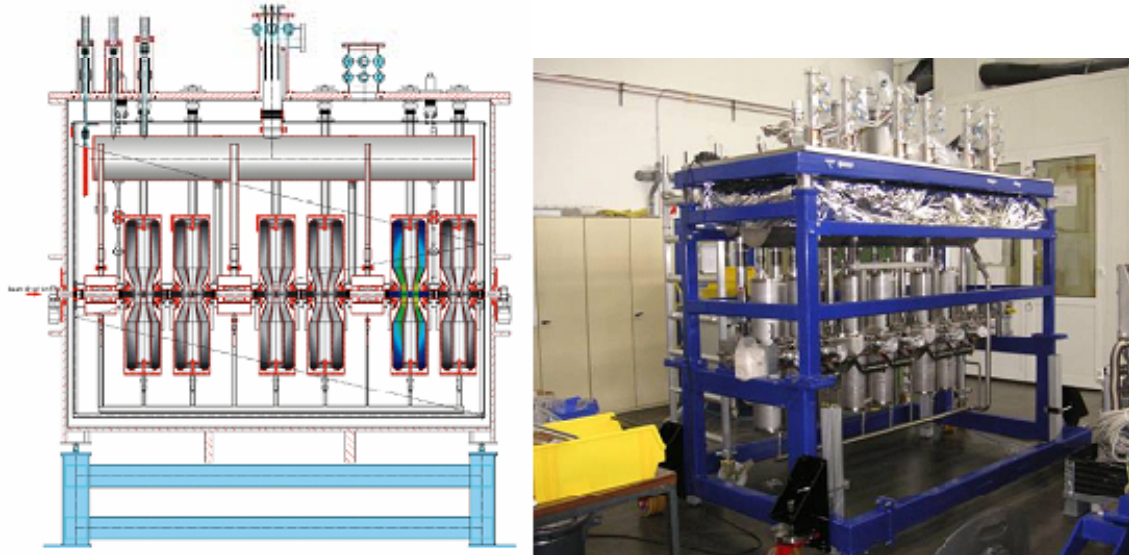Figure 5.6. Accelerating field profile on axis in the β=0.09 (left) and β=0.16 HWR EURISOL cavities.

Figure 5.7. The SARAF cryostat with separate vacuum. Right: cryostat under assembly [10].

5.2.3 Cryomodules

Different types of low-β cryomodule design might fit the EURISOL needs. In this paragraph different options will be discussed in order to assess a possible baseline choice.

5.2.3.1 General considerations on the low-β cryomodule technology

The cryomodule design is strongly influenced by the choice of vacuum system. In high-β cryomodules the elliptical resonators are substantially enlarged sections of beam pipes, and the beam vacuum is separated from the thermal isolation vacuum in a very natural way by the helium vessel which is built around the cavity. In low-β cryomodules for heavy ion accelerators, however, this separation is usually not applied and the cryomodule design, that includes numerous cavities and accessories, is considerably simplified. This results in a lower cryomodule cost and larger space available in the cryostats. New projects of low-β linacs for cw high intensity, low-β ion beams have

chosen separate-vacuum cryomodules [3] [4] [23]. The SARAF cryostat is the first one already under commissioning equipped with Half-wave resonators, rf lines and couplers which are close to the EURISOL specifications (Fig. 5.7). The IFMIF-EVEDA cryostat has an innovative structure for HWRs with a very compact, cylindrical vacuum tank. The HWR sit in horizontal position, allowing to place the long, 200 kW rf power couplers in vertical position from the bottom of the cryostat. However, a similar cryostat could allow also vertical HWRs like the EURISOL ones (Fig. 5.8). These separate-vacuum cryostats could also fit the EURISOL requirements. The main advantage of separate vacuum is the possibility to access components inside the cryostat without breaking the beam line vacuum, thus preserving cleanliness of the resonators rf surface. For a long time, common vacuum was thaught to cause transfer of contaminants from the cryostat volume to the extremely clean cavity interior, thus cavity performance degradation. More recently, however, reliable operation at highest gradient was demonstrated for quarter-wave resonators in common-vacuum cryomodules, with no degradation even after cryostat venting [22].

One disadvantage of separate vacuum is the necessity of two different vacuum systems; pumping inside resonators must be done through relatively long pipes with high impedance. In common vacuum, the cavities are pumped through the beam ports and the cryostat volume, with significantly lower impedance. Another disadvantage of separate vacuum is the necessity of mounting vacuum-tight bellows between all neigbouring components, requiring additional space for bellows and flanges. All Rf feedthroughs must be duplicated in separate vacuum cryostats in order to pass through two different vacuum barriers, with cost increase and mechanical complication. This is not the case for common vacuum. In common vacuum the space between components can be limited, or used for other purposes (e.g. to place stripline BPMs) and the mounting procedure is simplified. The absence of bellows between cavities and cryostat walls, moreover, improves thermal insulation.

It was demonstrated that no contaminant can be transferred when the cryostat is in vacuum, and a clean assembly procedure (required also in separate-vacuum cryomodules) prevents accumulation inside the cryostat of possible contaminants that could be mobilized in case of venting.
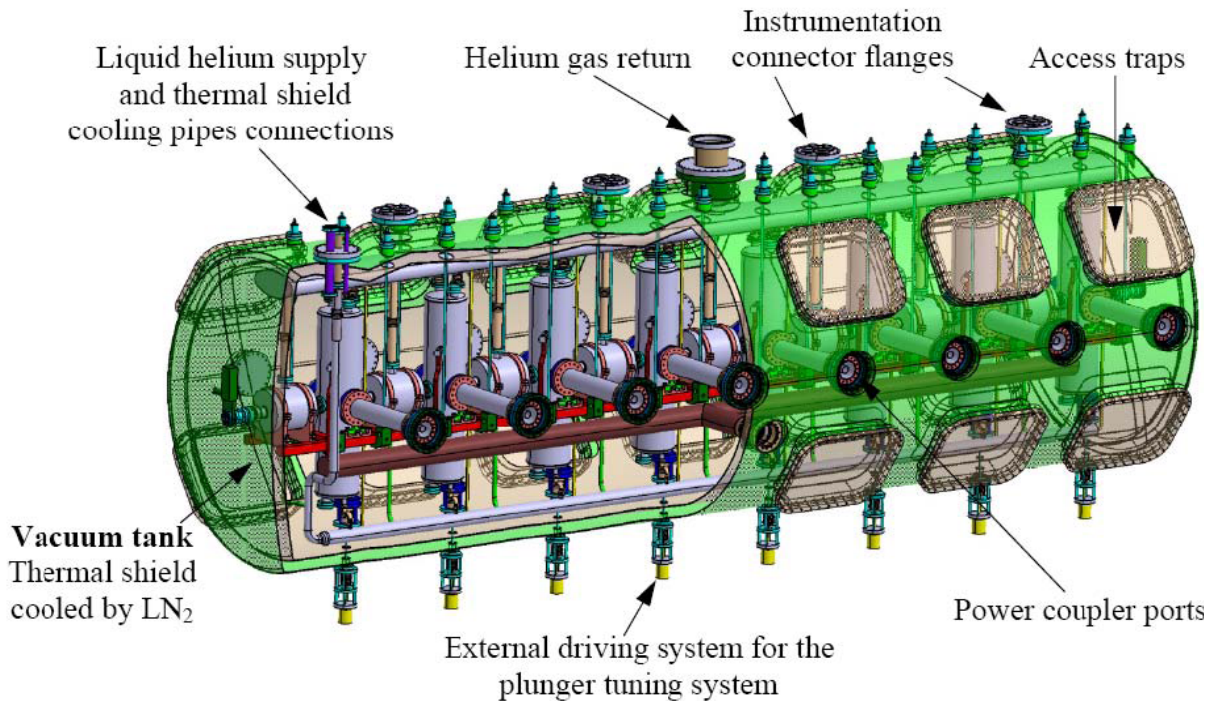

Figure 5.8. The IFMIF-EVEDA cryostat designed for HWR resonators vertical positioning [4].

A consequence of these recent results is that the choice of vacuum design should not be anymore dictated by performance expectations, since the most performing low-β cavities operate presently with common-vacuum, but by other considerations.

The tecnology of low-β cryomodules with common-vacuum was mainly developed for heavy ion linacs. Best results in operation have been obtained at TRIUMF in common vacuum cryostats with outer shield cooled with liquid Nitrogen, used also for cooling also rf power couplers (Fig. 5.9).

The operation temperature of choice, at 176 MHz, is the standard liquid He temperature of 4.2÷4.5 K. The BCS surface resistance of Niobium, at that frequency, is about 8 nΩ, comparable to the residual resistance expected in operating HWRs and SPOKE cavities. The little advantage in rf power losses that could be achieved using superfluid Helium would be more than counterbalanced by the loss of efficiency in Helium production and by the increased cost of the cryogenic system. However, the presence of a large cryogenic system for 2.2K liquid Helium required for the high-β elliptical cavity might change this view and suggest the use of this temperature also for the SPOKE cavities.

Stability of the Helium pressure in the cryomodule is critical for resonators operation. Excellent stability of ±1 mBar is nowadays achieved in many cryogenic systems for superconducting linacs working at 4.2K. This value must fit the resonator frequency response to pressure and its design rf bandwidth. In the case of EURISOL, the loaded Q of the low-β cavities is about 10^6, determined by the required beam loading, and the 3 dB rf bandwidth is about 200 Hz. For reliable operation, the resonator frequency response to pressure fluctuations and to Lorentz force detuning must be well below this value. The calculated values for the EURISOL cavities (Table 5.3) fit this requirement with a large safety margin. Different possibilities are available for the HWR cryostats. When the EURISOL DS project started, no HWR of this type was available. Nowadays, at least 2 projects under construction (SARAF and IFMIF-EVEDA) make use of HWRs with similar frequency and beta, operated in separate vacuum. The present SARAF β=0.09 cavities are in the commissioning phase, and the IFMIF cavities are in the prototype design stage. In the future, a simple alternative for EURISOL might be the adoption of the full package of SARAF or IFMIF cryomodules with separate vacuum and use them in the EURISOL HWR section, with some acceptable compromise. At present, however, no strong reason appears against common vacuum cryostats, both in terms of cost and performance, and EURISOL might take advantage of it.

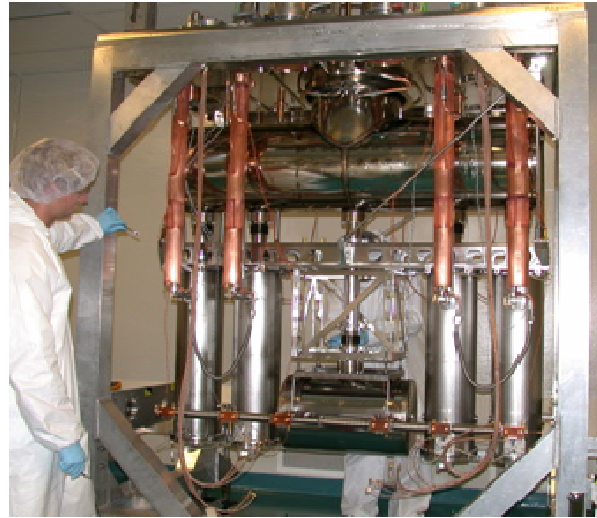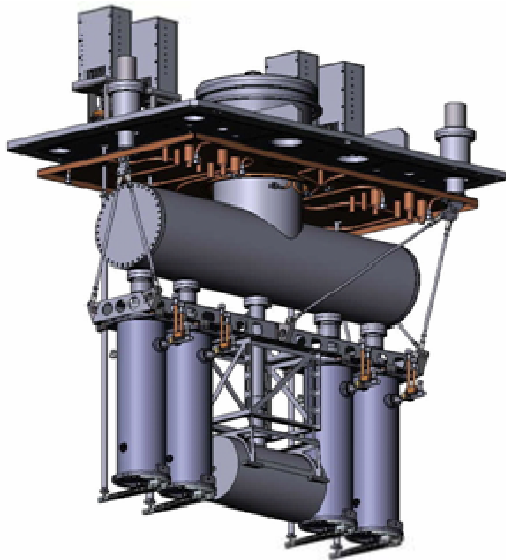Figure 5.9. Views of the TRIUMF-ISAC2 common vacuum cryostat hosting Quarter-wave resonators and superconducting solenoids [25].

5.2.3.2 EURISOL HWR cryostats

The possible design of a EURISOL HWR cryostat could be developed starting from the common vacuum ISAC-2 design [21], or from the previously described ones with separate vacuum. SARAF type cryostats, inspired by the ISAC-2 ones and modified for separate vacuum operation, would have rf power requirements and mechanical characteristics fitting well the EURISOL specifications. The main modifications that would be required are related to cryostat length, to the rf tuning system of the EURISOL HWRs (considerably lighter than the SARAF one), the vacuum system, which would consist of only one turbomolecular pump, and of course superinsulation, which would not be necessary anymore for common-vacuum. The larger number of resonators and solenoids, resulting in increased cryostat lengths, would require a reinforced mechanical design. In the IFMIF-EVEDA project, presently in the construction phase, cylindrical cryostats designed to contain 8 HWR cavities and 4 or 8 superconducting solenoids have been adopted. These cryostat could also be
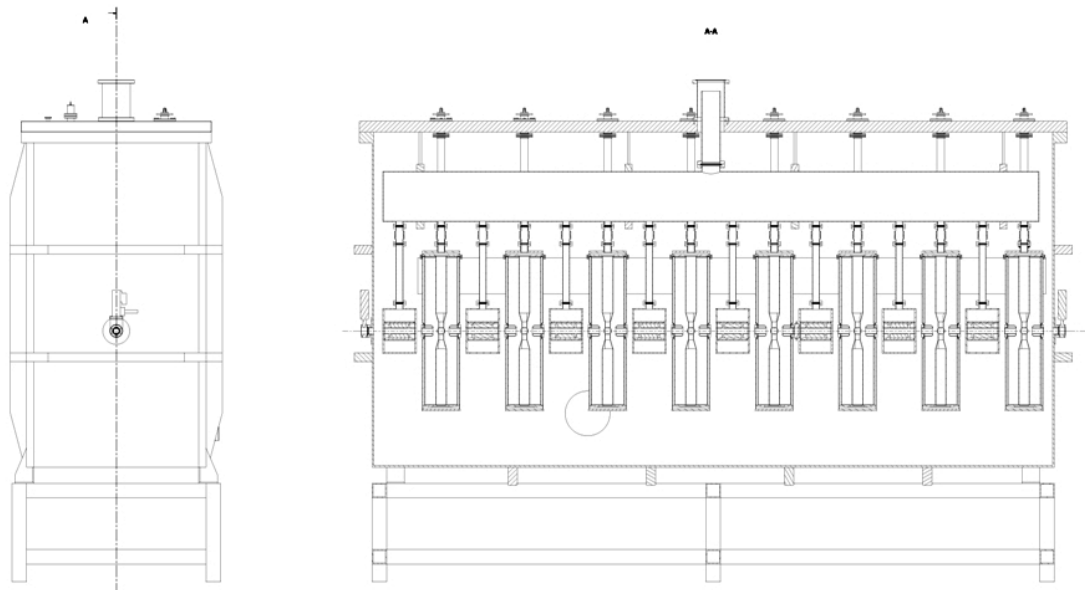
Figure 5.10. Sketch of the possible Low-β cryostat structure (HWR1 in the figure).

adapted to EURISOL for operation in common vacuum and with rf power lines downgraded to 10 kW levels.

Possible cryogenic characteristics, extrapolated from the calculated performance of the ISAC-2, low-β cryostats with common vacuum and liquid nitrogen shields (which includes 8 SC cavities +4 SC solenoids), are reported in table 5.4.

Table 5.4. Main specifications for the HWR cryostats

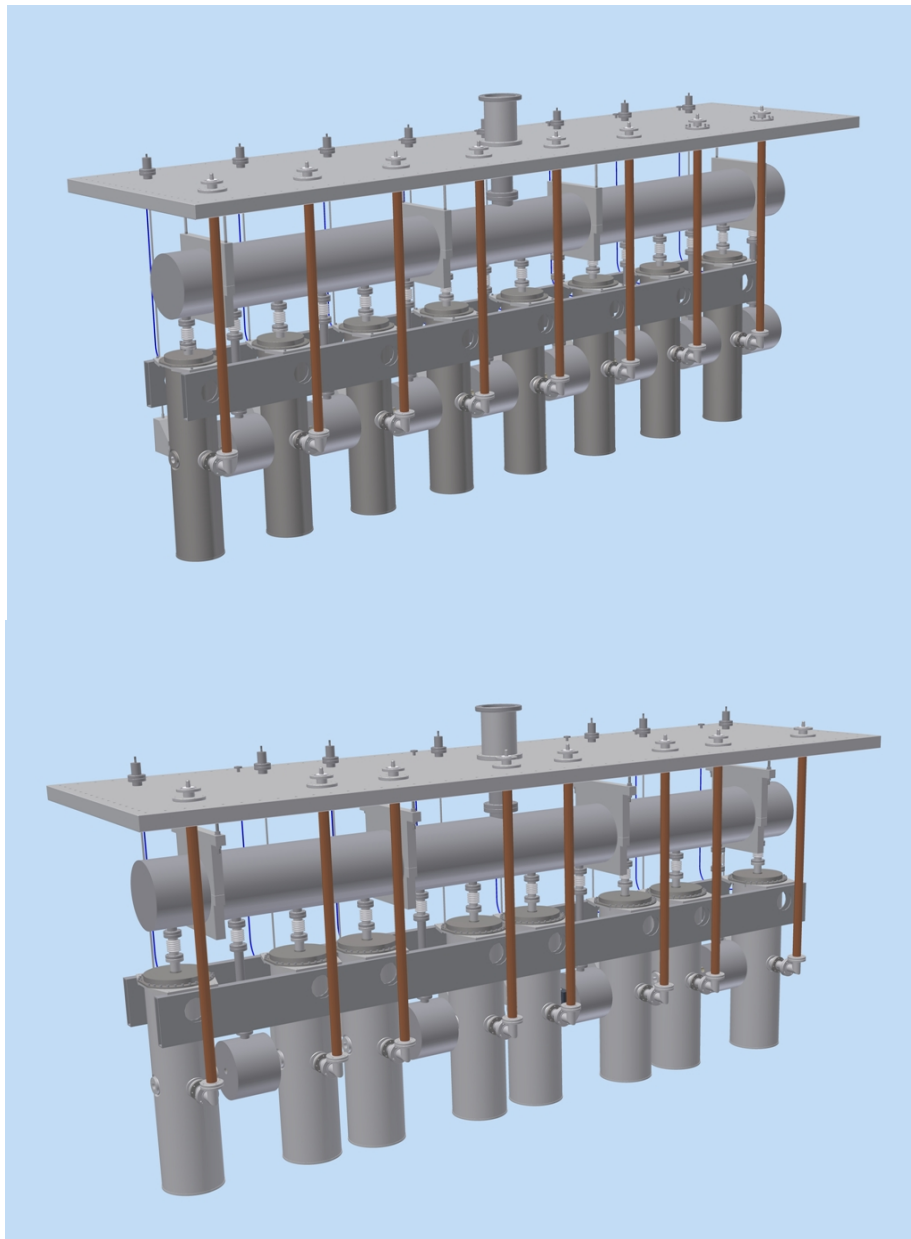| Cryostat type		β=0.09	β=0.16
Cryostat length	m	4	3.72
n. HWRs/cryo		8	8
n. solenoids/cryo		8	4
Operation T	K	4.2÷4.5	
Dynamic load/HWR at 4.5K	W	10	
Dynamic load/rf coupler at 4.5K	W	1	
Static load /cryo at 4.5K	W	22	
Total load /cryo at 4.5K	W	110	

Figure 5.11. View of models of the interior part of possible EURISOL low-β cryostats with common vacuum. Top: HWR1 (β=0.09); Bottom: HWR2 (β=0.16).

Stripline beam position monitors can be accomodated inside cryostats in the space left between cavities and solenoids. This does not present severe problems in common vacuum cryostats since the BPM itself is only a few centimeters long, and additional space for bellows and vacuum-tight feedthroughs is not required. The low-β cryomodule is completed by a diagnostics box located after the cryostat.

5.2.3.3 Superconducting solenoids

The required SC solenoids are similar to the ones (although without steerers) used in the SARAF linac. Solenoids with 9 T field and steerers with 5×10^{-2} T·m, thus above the EURISOL specifications, have been designed for the RIA project [17]. SC solenoids with steerers have been prototyped and tested for the HINS project [20].
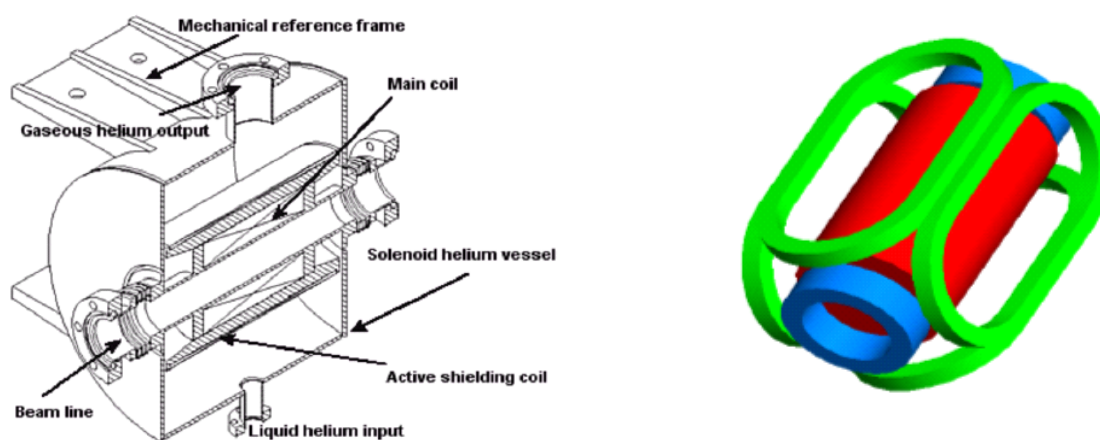

Figure 5.12. Left: Cut-out of the SARAF solenoid [26]. Right: schematic of a solenoid with bucking coils and racetrack steering dipole coils [17].

These solenoids include fringing field clamps (bucking coils) in order to keep the magnetic field below 10 µT at the resonator surface, and steering coils tested up to 10^{-2} T·m. Another model, with 5 T solenoid field and 2.5×10^{-3} T·m steering dipole fields, is under development in the framework of the IFMIF project.

Each solenoid and each steerer requires a couple of high temperature superconducting wires with current leads, cooled by He vapor. Thus each solenoid with horizontal and vertical steerers requires 6 current leads, that must be connected with the He recovery system. The required number of such special elements 2 per cryomodule.

5.2.3.4 Rf couplers

The rf coupler was developed in the Task 8 framework and is designed to allow at least 10 kW in any matching conditions. It fits the a $1^{5/8}$ ' port on the HWRs equator and allow operation at the nominal gradient and conditioning up to approximately twice this level.

The rf coupler lines inside the cryostats are coaxial ones with a 90° angle and similar to the ones used in the SARAF cryostats.
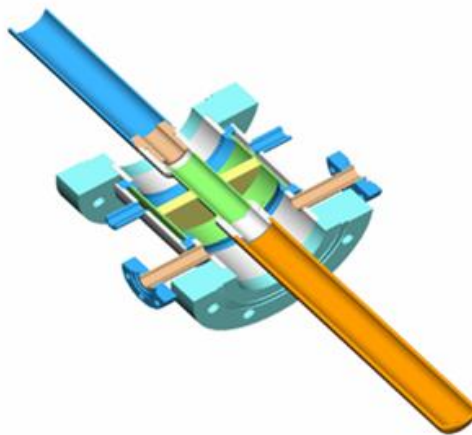

Figure 5.13. Sketch of the EURISOL rf coupler developed in the TASK8 framework.

RIDS 515768 TASK: 7	DATE: 3/2009	
DELIVERABLE: D3-LOW- AND MEDIUM-β LINAC	PAGE 58	

5.2.3.4 Rf amplifiers

Operation with superconducting cavities is characterized by nearly full reflection of the input power to the rf coupler in the absence of the beam, when the loaded quality factor almost completely determined by the coupling. In low current linacs with negligible beam loading, overcoupling is required in order to build a sufficiently large rf bandwidth to cover the entire detuning range caused by mechanical vibrations, Helium pressure fluctuations, Lorentz force detuning, etc. In highly beam loaded cavities, the rf bandwidth is usually wide enough to allow reliable control of phase and amplitude. However, in the EURISOL case that bandwidth is of the order of 200 Hz and this have shown to be rather critical in resonators with poor mechanical stability. The EURISOL HWRs should allow a safe control at full current. However, an extra rf power amount of at least 25% should be kept for reliable amplitude and phase control. For the MEBT bunchers, an extra 20% safety margin in the nominal accelerating gradient should be kept as well to leave some freedom in the beam parameters optimization; this puts further requirements to the available rf power for these normal conducting cavities. In SC cavities, the rf power reqirements are dominated by beam loading.

In the beam loading calculations, instead of the 5 mA required to the linac beam transport capability, the nominal EURISOL beam current has been taken. This current is 4 mA for protons, limited by the maximum nominal power allowed by neutron converters in high power targets. The HE splitter can feed three additional 200 kW beam lines for direct targets, giving a maximum beam current of 4.6 mA which determines the RF power amplifiers dimensioning. This implies a deuteron beam current capability of about 4.25 mA, and a final deuteron beam power on target of 1.15 MW.
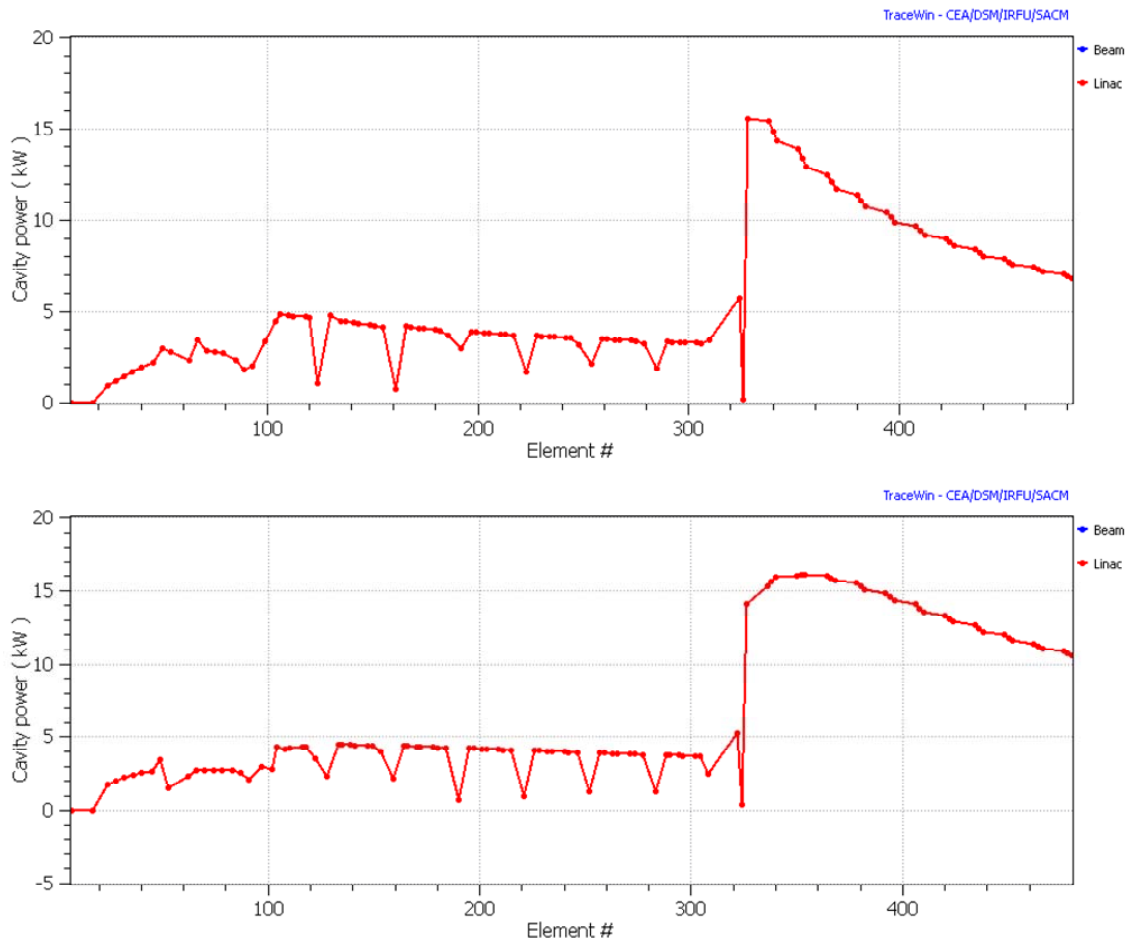
Figure 5.14. Beam loading in the resonators with the 4.6 mA H⁻ (top) the 4.25 mA D⁺ beams.

The beam loading of all the Low- and Mediun-β linac resonators are shown in Fig. 5.14, and the rf amplifier power requirements are shown in Table 5.5. These requirements can be largely fulfilled by the EURISOL 10 kW, unconditionally stable solid state amplifiers developed in the Task 8 framework [16]. This amplifier, developed for the 352 MHz frequency, has good linearity and efficiency, and can be operated with any matching condition, as required by superconducting resonator with large beam loading variability.

Table 5.5. Rf power requirements of the LMB resonators.

Resonator type		Buncher	HWR1	HWR2	3-Spoke
Rf frequency	MHz	176	176	176	352
Nominal operation gradient	MV/m	1	4.7	5.2	5.8
Rf power losses at max E_a	W	10^4	<10	<10	<10
Nominal max. beam loading	kW	0	4	5	16
Max. rf power requirements	kW	18	5	6.25	20

Two of these units can be coupled together by means of a 2-way 50 Ohm combiner and act as a unique, 20 kW amplifier for the Triple-Spoke resonators. The same amplifier design, with some modifications in the components to fit the new frequency, can be used for 10 kW units working at 176 MHz. The lower frequency allows a larger choice in the MOSFET type. The evolution of the characteristics of commercial components is very fast, and single amplifiers rated for 500 W cw at 176 MHz, compared to the 330 W that we have used, are already available.

Single 6.25 kW, 176 MHz units can be used for all the HWR cavities and for the first MEBT buncher (requiring 5 kW), while two combined 10 kW units can be used for Buncher 2. All rf power requirements wold be fulfilled with a large margin.

5.3 Medium-β linac

The technology of choice, for the medium-β section, is the 352 MHz triple-spoke resonators one. The main motivations are the following:

- A 4-gap cavity, compared to the 2-gap cavity of the HWR section, allows a sufficient velocity acceptance for $1 \leq A/q \leq 2$ in this linac section and, at the same time, a higher real-estate gradient;
- The only suitable 4-gap SC cavities, in this range of β and frequency, are of the SPOKE type;
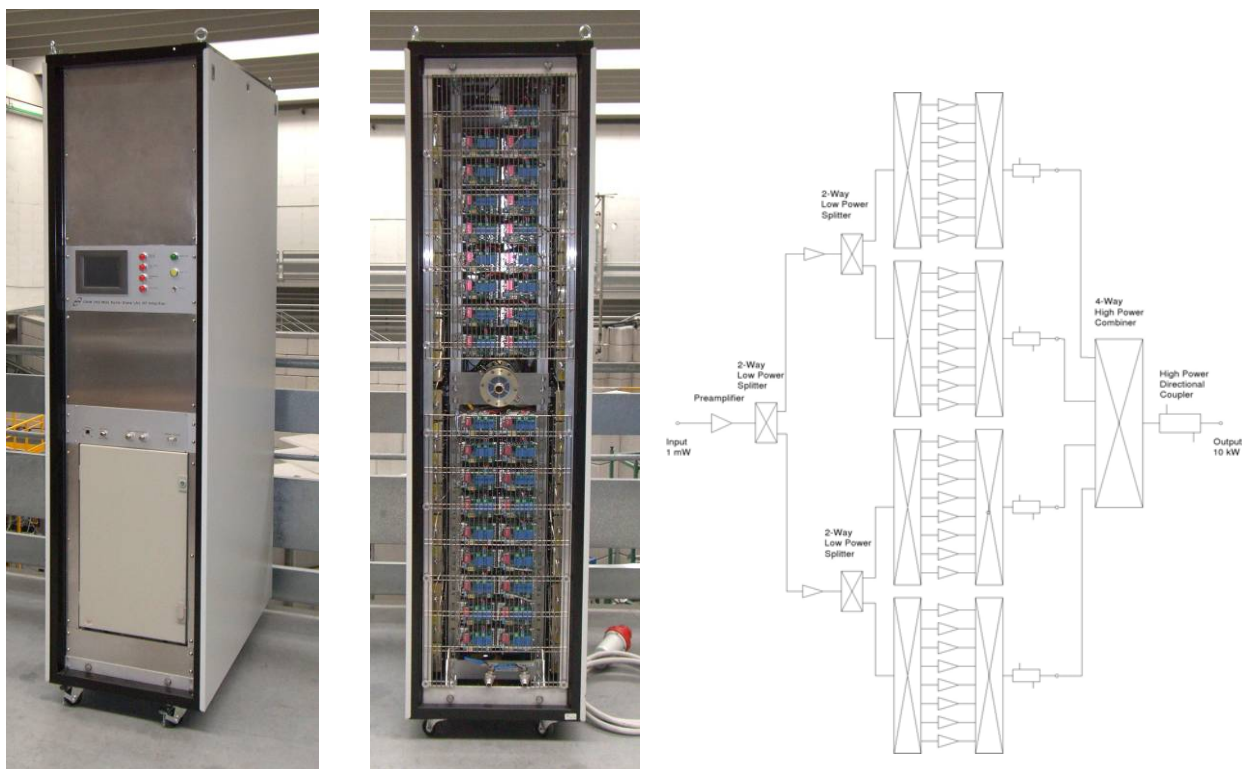
Figure 5.15 Left: The EURISOL 10 kW amplifier, front and rear views. Right: the rf amplifier block diagram.

- These resonators are rather compact and their housing in cryostat do not present particular complications;
- They are mechanically stable and easy to operate without need of fast tuning systems;
- Although never used in accelerators, several Spoke-type cavity prototypes have been developed for different applications in different laboratories, including EURISOL participants (IPNO), with excellent results.

The EURISOL Medium-β linac cryomodules have been developed in the Task 8 framework. The specific documentation is available in the Task 8 deliverables and will be omitted here to avoid duplications.

6. Conclusions

A new design of the EURISOL superconducting Low- and Medium-β linac has been studied. It replaces the original design that included two separate lines for protons and other ions. The present layout, characterised by injection at low energy with 176 MHz HWRs followed by 352 MHz Spoke resonators, and acceleration of both negative and positive ions, allows transport of all required beams in the same line, with considerable simplification of the linac structure and cost savings. The beam dynamics studies allowed to optimise the layout and to evaluate preliminarly the beam losses and the tolerable errors, showing that low loss transport can be achieved and that the EURISOL driver requirements are met. The tecnology suitable for the linac construction has been examined with special attention to critical components. Buncher resonators, HWR cavities and SPOKE cavities have been designed for this linac in synergy with EURISOL Task 8.

The study assessed the capability of the EURISOL Low- and Medium-β linac design to meet specifications.

References

[1] A. Facco, A. Balabin, R. Paparella, D. ZenereD. Berkovits, J. Rodnizki, J. L. Biarrotte, S. Bousson, A. Ponton, R. Duperrier, D. Uriot, V. Zvyagintsev, "BEAM DYNAMICS STUDIES ON THE EURISOL DRIVER ACCELERATOR", Proc. of LINAC08, Vancouver, Canada, 2008.

[2] Y. Blumenfeld; P. Butler; J. Cornell; G. Fortuna; M. Lindroos, "EURISOL Design Study: Toward the Ultimate ISOL Facility for Europe", Nuclear Physics News, Volume 19, Jan. 2009, pages 22-27.

[3] A. Nagler, D. Berkovits, I. Gertz, I. Mardor, J. Rodnizki, L. Weissman, K. Dunkel, F. Kremer, M. Pekeler, C. Piel, P. vom Stein, THE SARAF CW 40 MEV PROTON/DEUTERON ACCELERATOR", Proc. of LINAC08, Vancouver, Canada, 2008.

[4] A. Mosnier, A. Ibarra, A. Facco, "THE IFMIF-EVEDA ACCELERATOR ACTIVITIES", Proc. of EPAC08, p.3539.

[5] M. Kelly, "STATUS OF SUPERCONDUCTING SPOKE CAVITY DEVELOPMENT", Proc. of SRF2007, Beijing, China, 2007.

[6] J. Staples, D. Oshatz, T. Saleh, "Design of the SNS MEBT", Proc. of the 20th Linac Conf., Monterrey, CA, 2000.p. 250.

[7] BPMs

[8] S. Bousson et al., Proc. of LINAC 06, Knoxville, Tennessee, 2006, p. 706.

[9] A. Facco et al., PRST-AB 9, 110101 (2006).

[10] M. Pekeler, K. Dunkel, C. Piel, P. vom Stein, Proc. of LINAC06, Knoxville, Tennessee, USA, p. 321.

[11] R. Duperrier, N. Pichoff, and D. Uriot, in Proceedings of the International Conference Computational Science, Amsterdam, 2002.

[12] P.N. Ostroumov and V.N. Aseev, TRACK version 35 Simulation Code, Argonne National Laboratory, August 30, 2005.

[13] General Particle Tracer (GPT), Release 2.7, Pulsar Physics Ltd., The Netherlands, 2005. http://www.pulsar.ne.

[14] R. Duperrier et al. PRST-AB 10, 084201 (2007).

[15] J. Rodnizki, Proc. of LINAC06, Knoxville, Tennessee, USA, p. 426.

[16] F. Scarpa, D. Zenere, A. Facco, "STATUS OF THE HIGH POWER, SOLID-STATE RF AMPLIFIER DEVELOPMENT AT LABORATORI NAZIONALI DI LEGNARO", proc. EPAC 2008

[17] P. Ostroumov et al., "A NEW GENERATION OF SUPERCONDUCTING SOLENOIDS FOR HEAVY-ION LINAC APPLICATION", Proc. of LINAC 2002, Gyeongju, Korea, p. 332.

[18] T. Wangler, "PRINCIPLES OF RF LINEAR ACCELERATORS", John Wiley & Sons, 1998.

[19] A. Facco et al., "Completion of the PIAVE high energy buncher HEB1", INFN-LNL Ann. Rep. 2002

[20] I. Terechkine et al., "FOCUSING SOLENOIDS FOR THE HINS LINAC FRONT END", Proc. of LINAC08, Vancouver, Canada, p. 82.

[21] G. Stanford et al., "Engineering and Cryogenic Testing of the ISAC-II Medium Beta Cryomodule", Proceedings of LINAC 2004, Lübeck, Germany, p. 630.

[22] R.E. Laxdal, K. Fong, M. Laverty, A. Mitra, Q. Zheng, V. Zvyagintsev "RF CAVITY PERFORMANCE FOR THE ISAC-II SUPERCONDUCTING LINAC", Proc. of SRF2007, Beijing, China.

[23] A. Mosnier, "SPIRAL 2 : A HIGH INTENSITY DEUTERON AND ION LINEAR ACC ELERATOR FOR EXOTIC BEAM PRODUCTION", Proc. of PAC 2003, Portland, OR, USA, p. 595.

[24] R. Laxdal et al., "RECENT PROGRESS IN THE SUPERCONDUCTING RF PROGRAM AT TRIUMF/ISAC", Proc. of SRF2007, Beijing, China.

[25] R.E. Laxdal, et al, "Magnetic Field Studies in the ISAC-II Cryomodule", Physica C 441 (2006) 225-228.

[26] M. Pekeler, K. Dunkel, R. Henneborn, C. Piel, M. Poier, P. vom Stein, H. Vogel , "DESIGN OF A SUPERCONDUCTING HALF WAVE RESONATOR MODULE FOR PROTON/DEUTERON ACCELERATION", Proc. of SRF2003, Lubeck, Germany.

[27] A. Facco, D. Berkovits, R. Paparella and I. Yamane, Phys. Rev. ST Accel. Beams 10, 091001 (2007).

[28] The EURISOL Report – A FEASIBILITY STUDY FOR A EUROPEAN ISOTOPE-SEPARATION-ON-LINE RADIOACTIVE ION BEAM FACILITY – Appendix B, Edited by John Cornell, Published by GANIL B.P. 55027, 14076 Caen cedex 5, France. December 2003.